Maximal growth rate requires minimal metabolic complexity

Daan H. de Groot[1*], Coco van Boxtel[1], Robert Planqué[2], Frank J. Bruggeman[1], Bas Teusink[1]

***For correspondence:**
d.h.de.groot@vu.nl;
b.teusink@vu.nl

[1]Systems Bioinformatics, Vrije Universiteit Amsterdam, Amsterdam, The Netherlands;
[2]Mathematics, Vrije Universiteit Amsterdam, Amsterdam, The Netherlands

Abstract Natural selection pushes microbes towards maximal reproductive rates. This requires optimal tuning of metabolism, within biophysical bounds. A metabolic network can be decomposed into independent pathways, called Elementary Flux Modes (EFMs). Although billions of EFMs exist in a metabolic network, experiments suggest that few are simultaneously used. We present an extremum principle: metabolic simplicity is a consequence of rate maximisation. The number of used EFMs is determined only by the number of constraints that limit enzyme concentrations, not by the size, kinetics or topology of the network. Since the biochemical basis and biophysical constraints are similar across unicellulars, our theory explains why microorganisms show common metabolic behaviours, such as overflow metabolism. We present the extremum principle in a graphical framework, which also provides guidelines for experimental characterization of the growth-limiting constraints. This work provides a practical theory, rooted in biochemistry, that describes a fundamental limit of evolution and phenotypic adaptation.

Introduction

Fitter microorganisms drive competitors to extinction by synthesising more viable offspring in time (***Sæther and Engen***, 2015; ***Kussell and Leibler***, 2005). The rate of offspring-cell synthesis per cell, i.e., the specific growth rate, is a common determinant of evolutionary success across microbial species (***Sæther and Engen***, 2015). A high growth rate requires high metabolic rates, which in turn require high enzyme concentrations (***Cornish-Bowden***, 2014). Due to limited biosynthetic resources, such as ribosomes, polymerases, energy and nutrients, the expression of any enzyme is at the expense of others (***Basan et al.***, 2015; ***Molenaar et al.***, 2009). Consequently, the selective pressure towards maximal growth rate requires the benefits and costs of all enzymes to be properly balanced, resulting in optimally-tuned enzyme expressions (***Alon et al.***, 1999; ***Berkhout et al.***, 2013; ***Keren et al.***, 2016).

Tuning all enzyme expression levels appears to be a highly complex task. First, the metabolic network of a microorganism comprises hundreds to thousands of reactions with associated enzymes. Second, a change in expression level of one enzyme not only affects the rate of its associated reaction, but also changes intracellular metabolite concentrations. These metabolite concentrations influence the activities of many other enzymes in a non-linear fashion. In mathematical terms, microorganisms thus have to solve a high-dimensional non-linear optimization problem.

In contrast, experiments on many different microorganisms often show simple linear relations between growth rate, enzyme expression levels and metabolic rates (***Scott et al.***, 2014; ***Monod***, 1949; ***Klumpp et al.***, 2009), and the data can often be described by coarse-grained linear models (***Bosdriesz et al.***, 2015). This suggests that microorganisms in fact only use few regulatory degrees of freedom for tuning metabolic flux and protein expression. It is currently unclear why this simple,

low-dimensional behaviour results from the a priori enormously complicated tuning task. Given that the tendency towards simplicity is widespread amongst microorganisms, we expected this to be due to a general –evolutionary– principle.

We found an evolutionary extremum principle: growth-rate maximization drives microorganisms to minimal metabolic complexity. We provide the mathematical proof of this principle in the supplemental information (***Appendix 2***). It is derived from basic principles, more specifically from (i) mass conservation, *i.e.* steady-state reaction-stoichiometry relations, and (ii) enzyme biochemistry, i.e., the proportionality of enzyme activity with the amount of enzyme and its dependence on substrate and product concentrations. Our results provide a novel perspective on metabolic regulation, one in which the complexity is not determined by the size of the network or the rate equations, but by the constraints acting on the enzyme concentrations.

Results

The number of active Elementary Flux Modes is a measure of metabolic complexity, and is typically very low

Metabolic complexity can be unambiguously quantified as the number of flux-carrying 'Elementary Flux Modes' (EFMs). An EFM is mathematically defined as a minimal subnetwork at steady state: it is a minimal set of thermodynamically feasible reactions that form a network from external sources to sinks (***Schuster et al.***, 2000). These metabolic subnetworks are given by the reaction stoichiometry only, and thus for their identification no kinetic information is needed. Because of the many combinations of parallel, alternative metabolic routes in metabolic networks, the total number of such EFMs in a network is in the hundreds of millions; the exact number depends on the network and the available growth nutrients (***Maarleveld et al.***, 2015). In general, any steady state flux distribution can be decomposed into positive linear combinations of EFMs (***Schuster et al.***, 2000). For example, since pure respiratory growth and fermentative growth are both EFMs, respirofermentative growth is not, as it can be decomposed.

We call an EFM a minimal unit of metabolic complexity because the ratios between the fluxes through all participating reactions are fixed, and therefore none of its reactions can be removed. Consequently, a microorganism that uses one EFM can only change all reaction rates with the same factor: there is only one regulatory degree of freedom, instead of many if all reaction rates could have been tuned separately. In this case, flux values can be described by only one straight line. This becomes more complex when the number of flux-carrying (active) EFMs increases. Using this knowledge, the number of active EFMs can be estimated from flux measurements.

We re-analysed data from carbon-limited chemostats and estimated the number of flux-carrying EFMs to be low, in the order of 1 to 3 (***Figure 1***). That microorganisms choose only a handful of EFMs out of billions of alternatives suggests that these alternatives are not evolutionarily equivalent, and only a small number has been selected. Which ones are selected depends on the costs and benefits of each EFM, which themselves depend on the enzyme kinetics and constraints, as we shall see.

Evolutionary rate maximization can only be studied in a kinetic model of metabolism with constraints on enzyme concentrations

Any metabolic network can be given by a stoichiometric matrix $\boldsymbol{N}$, indicating which metabolites are consumed or produced in each reaction. A steady-state flux distribution is given by a vector of reaction rates $\boldsymbol{v}$ such that

$$\boldsymbol{N} \cdot \boldsymbol{v} = \boldsymbol{0}.$$

In steady state, we maximize the objective flux, which is one component of this flux vector. Often, the objective is chosen to be the (virtual) cell-synthesis reaction, also called the biomass reaction v_{BM}, which makes all cellular components in the right proportions according to the biomass composition (***Feist and Palsson***, 2010). Reaction rates are for almost all reactions given by

$$v_i = e_i k_{\mathrm{cat},i} f_i(\boldsymbol{x}),$$

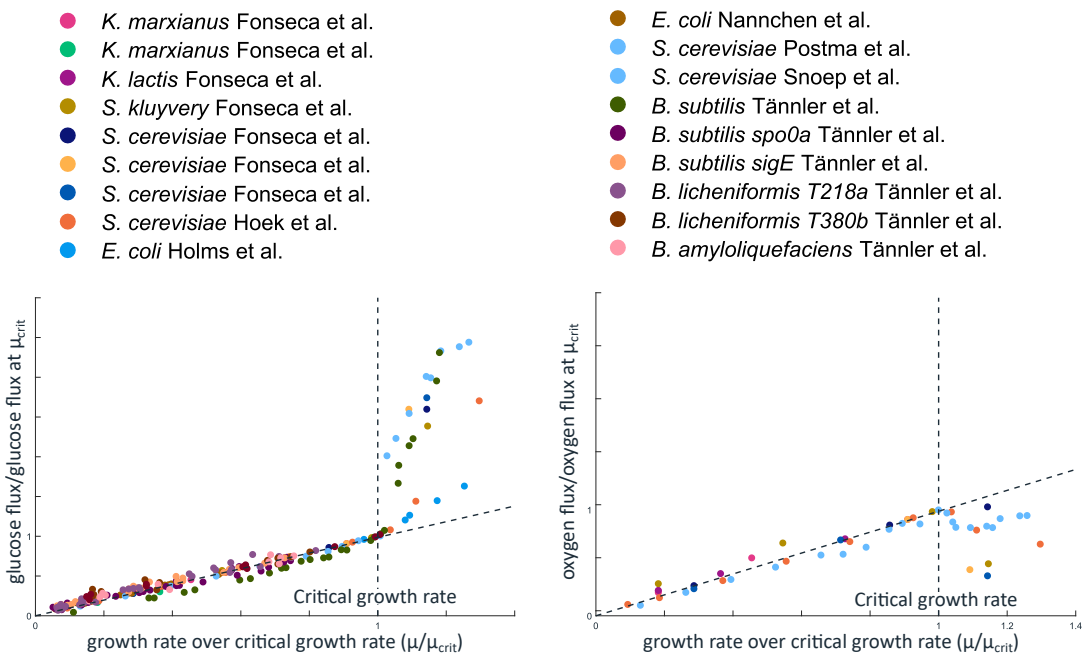

Figure 1. Proportionality of reaction rates and growth rates, shown by many microorganisms, are an indication of low metabolic complexity. Measured uptake rates (***Fonseca et al.***, 2007; ***Holms***, 1996; ***Nanchen et al.***, 2006; ***Postma et al.***, 1989; ***Snoep et al.***, 2009; ***Tännler et al.***, 2008) were gathered from experiments in which growth rate was varied in carbon-limited chemostats. For each species we normalized the measured growth rate to the so-called critical growth rate: the growth rate at which the production of overflow products starts. Uptake rates were normalized relative to the uptake rate of the species at the critical growth rate. Up to the critical growth rate, all microorganisms show a simple proportional relation between the growth rate and uptake rates of glucose and oxygen. After the critical growth rate, the reaction rates are no longer proportional, a phenomenon called overflow metabolism.

where e_i is the concentration of the enzyme catalyzing this reaction, $k_{\text{cat,i}}$ is its maximal catalytic rate and $f_i(\boldsymbol{x})$ is the saturation of the enzyme which is dependent on metabolite concentrations $\boldsymbol{x}$. The enzyme saturation $f_i(\boldsymbol{x})$ is often a non-linear function that potentially includes thermodynamic driving force, product inhibition, allosteric feedback and other enzyme-specific effects.

The maximization of the cell-synthesis flux is often modelled by stoichiometric methods (*e.g.*, through Flux Balance Analysis), in which additional constraints on reaction rates are imposed. However, such constraints do not reflect the ability of microorganisms to adapt: any reaction rate could in principle be increased by increasing the corresponding enzyme's concentration. However, bounds exist for enzyme concentrations, originating for example from limited solvent capacities of cellular compartments, or from a limited ribosomal protein synthesis capacity. These biophysical limits impose constraints that can each be modelled by a weighted sum of enzyme concentrations:

$$\sum_i w_i^{(j)} e_i \leq 1.$$

These constraints correspond to limited enzyme pools, because overexpression of one enzyme must be at the expense of others that are subject to the same biophysical constraint; the weights, $w_i^{(j)}$, determine the fraction that one mole/liter of the ith enzyme uses up from the jth constrained enzyme pool. For example, for a constraint describing the limited solvent capacity of the membrane, the weight of an enzyme is the fraction of the available membrane area that is used up by this enzyme; this weight is thus nonzero only for membrane proteins. We call a constraint 'active' when it limits the cell in increasing its growth rate, indicating that the corresponding enzyme pool is fully used. One enzyme can belong to one, several or none of these limited pools.

The number of constraints and the exact value of the weights may vary per organism. In general we expect this number to be low, and not many enzyme expression constraints have yet

been proposed in the literature. Many aspects of microbial growth have indeed been successfully described using constraints that are (or can be reformulated as) enzyme expression constraints, like limited catalytic rates and limited solvent capacities within cellular compartments (***Scott et al.***, 2014; ***Weiße et al.***, 2015; ***Basan et al.***, 2015; ***Hui et al.***, 2015; ***Molenaar et al.***, 2009; ***Scott et al.***, 2010; ***Vazquez and Oltvai***, 2016; ***Zhuang et al.***, 2011). In eukaryotes, with many more cellular compartments, the number of constrained protein pools may be larger than in prokaryotes.

If we introduce enzyme kinetics we can rewrite the enzyme constraints as:

$$\sum_i \frac{w_i^{(j)}}{k_{\text{cat},i} f_i(\boldsymbol{x})} v_i \leq 1.$$

We indeed see that these constraints are not equivalent to the flux constraints used in FBA, since the weighted sums depend on metabolite concentrations. To maximize the cell-synthesis flux, not only the enzyme concentrations should be optimized, but also the intracellular metabolite concentrations. Due to the neccessary inclusion of enzyme kinetics, flux maximization is turned into a complicated nonlinear problem. This is the problem we have investigated. We found that the solution uses a limited number of EFMs, which is perhaps suprising as these EFMs are themselves constructs based on stoichiometry only. As we will see, the enzyme kinetics set the costs and determine which (mixture of) EFM(s) is optimal, while the number of EFMs in the mixtures is set by the protein expression constraints, through the extremum principle.

The extremum principle: The maximal metabolic complexity is determined by the number of constraints on enzyme expression

In mathematical terms the extremum principle states: when the rate of a particular reaction in a metabolic network is maximized, the number of flux-carrying EFMs is at most equal to the number of constraints on enzyme concentrations that limit the objective flux. This is the basis of our finding that maximal growth rate requires minimal metabolic complexity, and this extends the result that rates are maximized by one EFM under a total protein constraint – one active enzyme constraint, therefore (***Wortel et al.***, 2014; ***Müller et al.***, 2014). In particular, the principle holds for the cell-synthesis reaction. Therefore, if the number of active constraints is low, so is the number of active EFMs at maximal growth rate.

The minimization of metabolic complexity can be illustrated by comparing the enzyme costs of all EFMs in the low-dimensional 'constraint space' defined by the limited enzyme pools (***Figure 2***). Because each reaction rate is proportional to its enzyme concentration, we can rank all EFMs (or mixtures thereof) by comparing the fractions of the limited enzyme pools that the EFMs use for reaching one unit of specific growth rate. Since an EFM uses different fractions of all pools, its cost becomes a multidimensional variable. So, each EFM is assigned a 'cost vector' in constraint space: a cost vector quantifies, for each constrained enzyme pool, the fraction that an EFM requires for producing one unit of objective flux - here the cell-synthesis flux. The direction of a cost vector thus denotes which pool is used most by this EFM. Shorter vectors, corresponding to EFMs with lower enzymatic costs, will fit more often and will therefore produce a higher flux. Specific growth rate maximization becomes a geometric problem in constraint space: fit the largest possible multiple of cost vectors within the constraint space.

The extremum principle is illustrated in ***Figure 2*** for the case with two constraints. Both constrained enzyme pools can always be fully used up with two cost vectors (EFMs), not more. However, an EFM with a diagonal cost vector can make full use of both pools on its own: hence, the number of EFMs that maximize flux can also be less than the number of active constraints. Another instance in which only one EFM is optimal, is when all cost vectors lie above or below the diagonal. In this case, there is only one active constraint; the other pool does not limit the total possible flux of the system under these conditions. We have derived the necessary and sufficient conditions under which it is optimal to use EFMs in mixtures (***Appendix 5***). ***Figure 2*** also reflects that metabolite

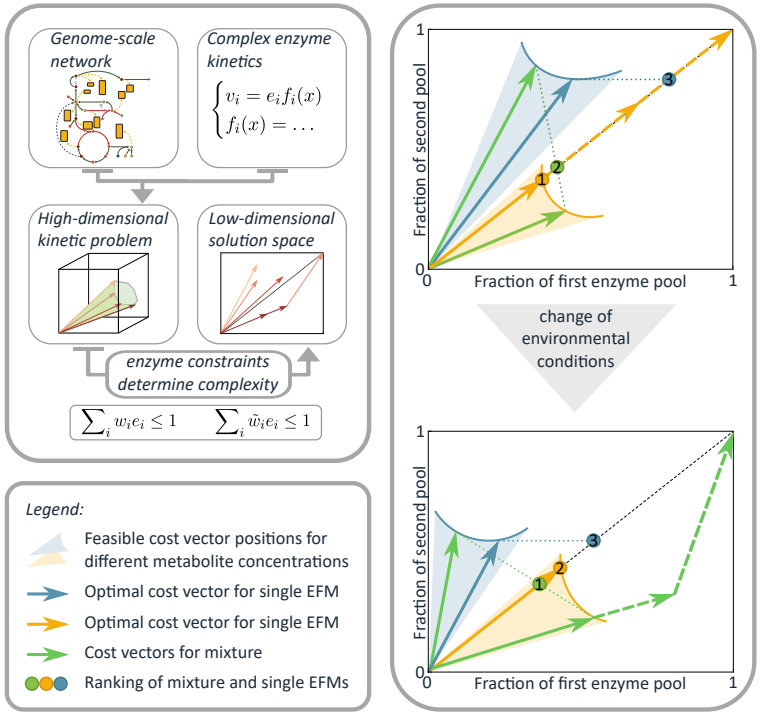

Figure 2. Illustration of the extremum principle and the cost vector formalism. Left panel: The extremum principle states that the dimensionality of the solution space is determined by the number of enzyme-expression constraints, rather than by the dimensionality of the metabolic network. The constraints result from biophysical limits, *e.g.*, limited solvent capacities within cellular compartments. **Right panel:** The *cost vector* $\boldsymbol{d}^i = [d_1^i, d_2^i]^\intercal$ of the ith EFM denotes the fractions of the first and second constrained enzyme pool that this EFM uses when producing one unit of objective flux. EFMs can be used in mixtures; we quantify the cell-synthesis flux produced by the EFM i by λ_i. The cost of mixing EFMs i and j corresponds to a weighted sum of the cost vectors: $\lambda_i \boldsymbol{d}^i + \lambda_j \boldsymbol{d}^j$. The mixture is feasible as long as none of the constraints is exceeded: $\lambda_i \boldsymbol{d}^i + \lambda_j \boldsymbol{d}^j \leq \mathbf{1}$. The optimum is achieved by maximising the sum of weights $(\lambda_i + \lambda_j)$. This solution is shown by the dashed vectors. The sole use of an off-diagonal cost vector leads to underuse of one constraint, while diagonal cost vectors can exhaust both constrained pools. A mixture of EFMs will always be a combination of an above-diagonal and a below-diagonal vector. All EFMs and mixtures thereof, can be ranked by a dot on the diagonal which denotes the average cost per unit cell-synthesis flux. Above-diagonal cost vectors should be projected horizontally on the diagonal, below-diagonal vectors vertically, and for mixtures the dot is at the intersection with the connecting line. The (mixture of) EFM(s) with the lowest average cost leads to the highest growth rate (the mathematical proof is included in ***Appendix 5***). The enzymatic costs of an EFM depend on the intracellular metabolite concentrations, *i.e.*, the saturation of enzymes. The shaded regions indicate alternative positions for the cost vectors at different intracellular metabolite concentrations, two of them are shown. The blue and orange cost vectors lead to the highest growth rate when using only that EFM. Upon a change of environmental conditions, the mixture of EFMs becomes better than either single EFM. This would lead to a change in metabolic behaviour.

concentrations affect the length and direction of the cost vectors via enzyme kinetics (depicted by the shaded areas). We study this metabolite-dependency in ***Appendix 5***.

The extremum principle holds regardless of the complexity of the metabolic network, *i.e.*, of its kinetics and its structure. The metabolic complexity is only determined by the number of active constraints; the kinetics and structure subsequently determine which EFMs are optimal and selected by evolution - as illustrated by *in silico* evolution of metabolic regulation towards only one active EFM (***Gottstein et al.***, 2014). For this reason, also genome-scale metabolic models, which contain all the annotated metabolic reactions that a microorganism's genome encodes (***Price et al.***, 2004), and even the ones that have been studied with different additional resource constraints (***O'Brien et al.***, 2014; ***Goelzer et al.***, 2015), behave qualitatively similar to simplified core models. Coarse-grained models can thus be used without loss of generality, which greatly facilitates our understanding of metabolic behaviour.

The number of enzymatic constraints can be inferred from experimental data: overflow metabolism is caused by two constraints

A well-known phenomenon observed in many microbes is overflow metabolism: it refers to the apparently wasteful excretion of fermentation products. Examples are the aerobic production of ethanol by yeasts (Crabtree effect), lactate by cancer cells (Warburg) or acetate by *Escherichia coli* (***Basan et al.***, 2015; ***van Hoek et al.***, 1998; ***Peebo et al.***, 2015). The onset of overflow metabolism is generally studied as a function of growth rate (*e.g.*, in chemostats where the growth rate is set by the dilution rate of the culture). Before some critical growth rate, cells fully respire, but when the growth rate is increased above some critical value, respiratory flux decreases and the flux of overflow metabolism emerges.

Interpretation of data of overflow metabolism with the extremum principle at hand, immediately reveals that an additional enzymatic constraint must have become active at the critical growth rate (see ***Figure 1***). Below the critical growth rate, the respiratory flux is proportional to the growth rate, which is a characteristic of single EFM usage (see ***Appendix 8***). Above the critical growth rate however, the decreasing respiratory flux and increasing fermentation flux indicate that at least two EFMs and therefore two constraints must be active.

We gain more insight by applying the cost vector formalism on a coarse-grained model of overflow metabolism (Figure ***Figure 3***). The model includes a respiration pathway and an acetate overflow branch. All steps include enzyme kinetics, and constraints are imposed on two enzyme pools: total cytosolic protein, and total membrane protein. Although experimentally the growth rate is set by the dilution rate of the glucose-limited chemostat, growth rate always correlates with the available glucose concentration. Therefore, we can here model overflow metabolism as a function of the glucose concentration. We see that this model can indeed explain overflow metabolism as the consequence of growth rate maximization. At low extracelullar glucose concentrations, all cost vectors have high membrane costs and lie above or at best at the diagonal (as the membrane constraint is on the y-axis): the membrane pool limits substrate uptake and therefore favours efficient use of glucose via respiration. In this respiratory regime, the cytosolic pool could be considered in excess. However, the expression of more cytosolic proteins can keep the intermediate metabolite concentration low and thereby increase the growth rate by reducing product inhibition of the transporter proteins. This may explain the apparent overcapacity of glycolytic enzymes under these conditions as observed in a number of microorganisms (***Goel et al.***, 2015; ***Canelas et al.***, 2011). Our core model predicts that, as extracelullar glucose concentrations increase, so does the saturation level of the glycolytic enzymes and flux can increase without a change in protein level (again as observed). Consequently, for a large range of external substrate concentrations pure respiration leads to maximal growth rate by fully exploiting the two available enzyme pools. The membrane constraint is however more growth-limiting, *i.e.*, loosening this constraint will give a larger growth rate benefit. At high glucose concentrations, transporters become more saturated (and cost vectors become shorter in the membrane direction) and the respiration cost vector

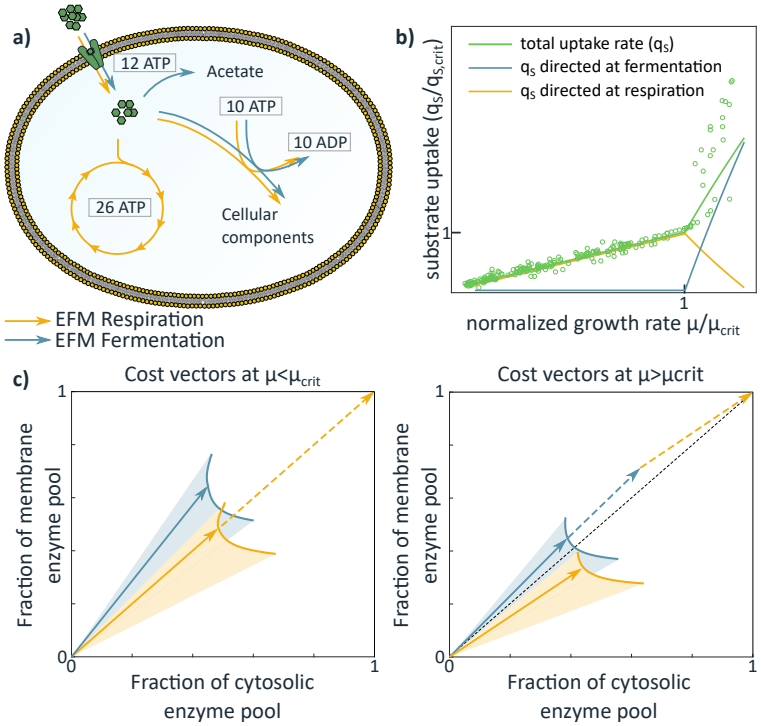

Figure 3. The cost vector formalism provides insight in how growth rate maximization leads to overflow metabolism. a) A core model with two EFMs that individually lead to cell synthesis (orange: respiration and blue: acetate overflow). All considered reactions have an associated enzyme, whose activity depends on kinetic parameters and the metabolite concentrations. We varied growth rate by changing the external substrate concentration. Given this external condition, the growth rate was optimized under two enzymatic constraints (limited cytosolic enzyme $\Sigma\, e_{i,\text{cyto}} \leq 1$ and limited membrane area $e_{\text{transport}} \leq 0.3$). **b)** The predicted substrate uptake fluxes directed towards respiration and fermentation are in qualitative agreement with the experimental data (shown before in ***Figure 1***) of several microorganisms scaled with respect to the growth rate (μ_{crit}) and uptake rate (q_{crit}) at the onset of overflow (***Basan et al.***, 2015; ***van Hoek et al.***, 1998; ***Peebo et al.***, 2015). **c)** The cost vectors (solid arrows) of the two EFMs before (left) and after (right) the respirofermentative switch. The position of the cost vectors are shown for the optimized metabolite concentrations; the shaded regions show alternative positions of the cost vectors at different enzyme and metabolite concentrations. The dashed vectors show the usage of the EFMs in the optimal solution.

becomes below-diagonal: pure respiration will leave the membrane protein pool underused, while the cytosolic pool limits respiration. A better strategy is to respire less and make some of the cytosolic pool available for another EFM that can exploit the underused membrane pool. The net outcome is that a mixture of EFMs attains a higher growth rate than either of the two EFMs alone.

We think that many published explanations of overflow metabolism are unified by the extremum principle. Indeed, we show in ***Appendix 4*** that explanations for overflow metabolism offered by other modelling methods, implementing different constraints, such as coarse-grained whole cell models (***Weiße et al.***, 2015; ***Molenaar et al.***, 2009; ***Basan et al.***, 2015) and constraint-based genome-scale M-models (***Vazquez and Oltvai***, 2016; ***van Hoek and Merks***, 2012; ***Mori et al.***, 2016; ***Nilsson and Nielsen***, 2016) are mathematically all instances (or simplifications) of the exact same constrained optimization problem that we study here: their maximizers thus all follow the extremum principle. So-called ME-models (***O'Brien et al.***, 2014) fall under a slightly different class of mathematical problems, but the onset of overflow metabolism is still caused by an additional active constraint. Our new insight is thus that all overflow models must use at least two constraints. However, since the above explanations all capture the phenomenon and solve the same mathematical problem, we cannot conclude on the mechanistic nature of the constraints, yet.

The identity of the enzymatic constraints can be revealed by experimental perturbations

Using the cost vector formalism we can predict the effect of experimental perturbations on metabolism. Examples of perturbations are the expression of non-functional proteins or the inhibition of enzymes, which can respectively be interpreted as reducing a limited enzyme pool, or lengthening the cost vectors. The effect of such perturbations on growth, when two EFMs are expressed, was analysed in the cost vector formalism (***Appendix 6***). With ***Figure 4*** we visualize two of such perturbations by reducing the size of the accessible area of constraint space. We here visualized perturbations as a reduction of the available area in constraint space, and study perturbations that lengthen the cost vectors in ***Appendix 7***. Conversely, experimental data from a perturbation experiment can be used to deduce which enzyme pools were affected. In ***Figure 4*****a-d** we predict the (qualitative) effect of reducing the accessible area in constraint space for two cases (i) reduction of both enzyme pools by the same amount; or (ii) reduction of only the first constrained pool. We subsequently compare these predictions with the perturbation experiments carried out by Basan et al. (***Basan et al.***, 2015) (see SI for a mathematical analysis).

The overexpression of the unused cytosolic protein LacZ coincides with our predicted effect of an equal reduction of two enzyme pools ***Figure 4*****e**. If one interprets the constraints as a membrane constraint and a cytosolic constraint, this is surprising at first, since LacZ is a cytosolic protein. However, the costs of making a cytosolic protein also includes membrane proteins, as protein synthesis requires (imported) free energy and nutrients. If LacZ can be considered an average protein in terms of resource requirements, and if metabolism was already tuned to optimally use both limited enzyme pools, all EFMs thus require more of both limited enzyme pools to maintain the growth rate (the cost vectors are lengthened). This is indeed equivalent to a symmetric reduction of the available area in constraint space.

An example of a perturbation that affects one enzymatic pool more than the other, is the addition of chloramphenicol (***Figure 4*****f**). Chloramphenicol inhibits translation and the cell therefore needs a larger number of ribosomes per unit flux. This again adds a cost for protein synthesis, thereby reducing both pools. The experiment however shows that chloramphenicol has a more dominant effect on the first pool (x-axis) than on the second pool (y-axis). This means that the increased number of ribosomes has an additional effect on the first pool, which could well be related to the large cytosolic volume that the ribosomes take up. Technically, the inhibition of translation could possibly lengthen the cost vectors of all EFMs in the x-direction to different extents. We study this case separately in ***Appendix 7*** and show that the effects are equivalent to the effects of resizing the first enzyme pool.

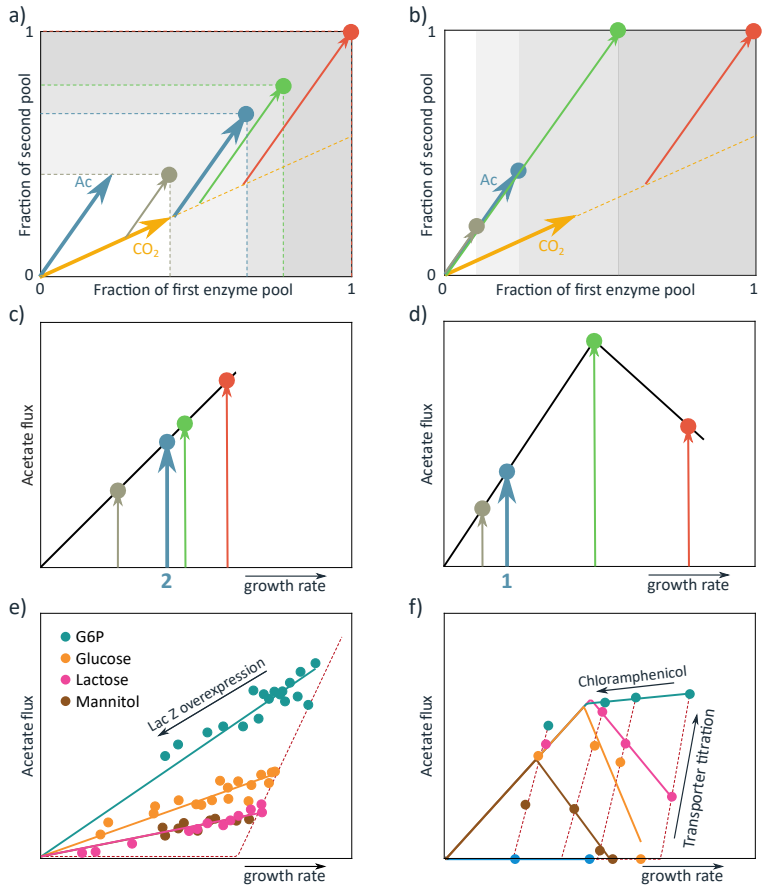

Figure 4. Predictions and experimental results of the perturbation of the size of limited enzyme pools during growth using a mixture of EFMs. a,c) Analysis of perturbations that tighten both protein pools with the same amount shows that flux and growth rate will decrease proportionally, as observed experimentally (**e)**) for the overexpression of LacZ on different carbon sources (data from Basan et al. (***Basan et al.***, 2015)). **b,d)** Perturbations that tighten an enzyme pool that is mostly used by one EFM (here denoted by CO_2) initially cause an increase in flux through the other EFM in the mixture(Ac). Eventually, at stronger limitations, this flux also decreases. **f)** This behaviour is observed, a.o., for translation inhibitor experiments using chloramphenicol (***Appendix 7***).

The perturbation experiments, and their analysis in the cost vector formalism, suggest a broadly-applicable experimental approach for testing candidate growth-limiting constraints. Given a candidate constraint, one could choose to perturb the size of the corresponding limited enzyme pool, *e.g.*, by the expression of a nonfunctional protein in this pool. The effect of this perturbation on the flux through the active EFMs can be compared with the predictions in **??**. This could validate or falsify whether certain limited enzyme pools are truly growth-limiting. One could also choose to inhibit a specific enzyme; this however introduces the risk of inhibiting some EFMs more than others, leaving the results potentially uninterpretable.

Discussion

The extremum principle that we derived and illustrated in this work predicts the evolutionary direction on a short timescale, dictating optimal enzyme expression levels. At a specific point in time, the extremum principle predicts that resources are reallocated to the most efficient enzymes at the expense of others that are less active per unit enzyme, *i.e.*, evolution reduces the number of active EFMs. On the longer timescale, kinetic parameters and network stoichiometry can evolve, thereby changing the evolutionary landscape, *i.e.*, evolution modifies the cost vectors. In this new landscape, the extremum principle will again predict minimal complexity, although the EFMs that are selected and the flux through these EFMs may have changed. Hence a microorganism selected by evolution will, in static conditions, only express a small number of EFMs and therefore its metabolism is low-dimensional. This could very well be the explanation of the simple linear relations that many experimentally measured relations show (***Scott et al.***, 2014; ***Monod***, 1949). This simplicity may also provide an explanation how only a few number of metabolites or proteins ("master regulators" such as CcpA or Crp) seem to regulate (central) metabolism (***Kochanowski et al.***, 2017).

While growth rate maximization leads to minimal metabolic complexity in static conditions, the metabolic network is still enormously versatile. An example in which such versatility is apparent is the simultaneous uptake of several carbon sources during growth (co-consumption). One could make the naive assumption that consumption of each substrate would represent the use of a specific EFM, and the co-consumption of a number of different substrates must therefore be due to an equal number of constraints. In *E. coli*, however, transport-mediated mixed substrate usage was observed in medium containing combinations of excess carbon sources (***Hermsen et al.***, 2015). Combinations of substrates that enter upstream of glycolysis with substrates that enter downstream often gave rise to a higher growth rate than can be reached on the substrates individually. We extended these experiments and experimentally found that *E. coli* cells do co-consume two carbon sources that enter upstream of glycolysis, or even three carbon sources (***Appendix 11***). This apparent contradiction was resolved by the analysis of a genome-scale metabolic network of *E. coli*, which showed that single EFMs exist that consume three carbon sources simultaneously. This shows that versatility arises from the large number of possible EFMs, of which only a few will be used.

Even though growth-rate maximization at constant conditions might at times be a rather crude approximation of the selective pressure, we expect the extremum principle to provide an 'evolutionary arrow of time'. When conditions change frequently, other aspects might come into play and fitness will be captured by the mean growth rate over environments, i.e., the geometric growth rate (***Sæther and Engen***, 2015). Whether extremum principles hold for the maximization of geometric growth rate is an open problem for future theoretical work.

The insight that the dimensionality of metabolism is bounded by the number of active constraints, reconciles earlier modelling approaches that have used resource allocation principles. Furthermore, we show that the same principles also hold for models that include enzyme kinetics and thereby metabolite dependencies. Many modeling approaches showed comparable shifts from respiration to (respiro)fermentation and mathematically they all fall under the same class of optimization problems, for which we derived the extremum principle. The kinetic self-replicator

model presented by Molenaar (***Molenaar et al.***, 2009), for example, does not show mixed strategies, but an abrupt switch between respiration and fermentation, testimony of a single active constraint. Although a membrane protein constraint was included, the size of cells could be freely adjusted to alleviate this constraint. In many studies with genome-scale stoichiometric models, mixed strategies do occur. Indeed in all these studies the glucose uptake flux was constrained (first constraint), in combination with some linear combination of fluxes that reflects the (second) constraint that was the focus of the study (solvent capacity, osmotic pressure (***Vazquez et al.***, 2008; ***Vazquez and Oltvai***, 2016), proteome limits (***Basan et al.***, 2015; ***Mori et al.***, 2016), membrane (***Zhuang et al.***, 2011; ***Szenk et al.***, 2018). Also in so-called ME (Metabolism and Expression) models (***O'Brien et al.***, 2014) and variants thereof (***Sánchez et al.***, 2017), growth rate is fixed and nutrient uptake is minimized. Again, overflow is observed in these models when an additional constraint (total proteome) is hit. We emphasize that mathematically any two constraints on different protein pools can lead to the same qualitative behaviour, as it does in these cited works.

The extremum principle is a null hypothesis about the course of a particular evolutionary process (***Smith***, 1978) which has direct operational implications for evolutionary engineering strategies. Increasing or decreasing the complexity of microbial metabolism might be desired, for example in industrial biotechnology where co-consumption of different sugars from biomass-hydrolysates are pursued, or prevention of overflow metabolism during heterologous protein production is attempted. Our extremum principle provides a species-overarching, molecular, constraint-based perspective on the systemic capabilities of biological networks and their contributions to microbial fitness.

Acknowledgments

We thank Sieze Douwenga, Willi Gottstein, Dennis Botman, Johan van Heerden, and Rinke van Tatenhove-Pel for comments, questions and proofreading. This work was supported by NWO VICI grant 865.14.005 and by NWO STAR grant 022.005.031.

References

Alon U, Surette MG, Barkai N, Leibler S. Robustness in bacterial chemotaxis. Nature. 1999 jan; 397(6715):168–171.

Basan M, Hui S, Okano H, Zhang Z, Shen Y, Williamson JR, Hwa T. Overflow metabolism in *Escherichia coli* results from efficient proteome allocation. Nature. 2015; 528(7580):99–104.

Berkhout J, Bosdriesz E, Nikerel E, Molenaar D, de Ridder D, Teusink B, Bruggeman FJ. How biochemical constraints of cellular growth shape evolutionary adaptations in metabolism. Genetics. 2013 jun; 194(2):505 LP – 512.

Bosdriesz E, Molenaar D, Teusink B, Bruggeman FJ. How fast-growing bacteria robustly tune their ribosome concentration to approximate growth-rate maximization. FEBS J. 2015; 282(10):2029–2044.

Canelas AB, Ras C, ten Pierick A, van Gulik WM, Heijnen JJ. An in vivo data-driven framework for classification and quantification of enzyme kinetics and determination of apparent thermodynamic data. Metab Eng. 2011 may; 13(3):294–306.

Cornish-Bowden A. Principles of enzyme kinetics. Elsevier; 2014.

Feist AM, Palsson BO. The biomass objective function. Curr Opin Microbiol. 2010; 13(3):344–349.

Fonseca GG, Gombert AK, Heinzle E, Wittmann C. Physiology of the yeast Kluyveromyces marxianus during batch and chemostat cultures with glucose as the sole carbon source. FEMS Yeast Res. 2007; 7(3):422–435.

Gagneur J, Klamt S. Computation of elementary modes: a unifying framework and the new binary approach. BMC Bioinformatics. 2004; 5(1):175.

Goel A, Eckhardt TH, Puri P, de Jong A, dos Santos F, Giera M, Fusetti F, de Vos WM, Kok J, Poolman B, Molenaar D, Kuipers OP, Teusink B. Protein costs do not explain evolution of metabolic strategies and regulation of ribosomal content: does protein investment explain an anaerobic bacterial Crabtree effect? Mol Microbiol. 2015; 97(1):77–92.

Goelzer A, Muntel J, Chubukov V, Jules M, Prestel E, Nölker R, Mariadassou M, Aymerich S, Hecker M, Noirot P, Becher D, Fromion V. Quantitative prediction of genome-wide resource allocation in bacteria. Metab Eng. 2015 nov; 32:232–243.

Gottstein W, Müller S, Herzel H, Steuer R. Elucidating the adaptation and temporal coordination of metabolic pathways using in-silico evolution. BioSystems. 2014; 117(1):68–76.

Gutnick D, Calvo JM, Klopotowski T, Ames BN. Compounds which serve as the sole source of carbon or nitrogen for Salmonella typhimurium LT-2. J Bacteriol. 1969 oct; 100(1):215–219.

Hermsen R, Okano H, You C, Werner N, Hwa T. A growth-rate composition formula for the growth of *E. coli* on co-utilized carbon substrates. Mol Syst Biol. 2015; 11(4):801.

van Hoek MJA, Merks RMH. Redox balance is key to explaining full vs. partial switching to low-yield metabolism. BMC Syst Biol. 2012; 6(1):22.

van Hoek P, Van Dijken JP, Pronk JT. Effect of Specific Growth Rate on Fermentative Capacity of Baker ' s Yeast. Society. 1998; 64(11):4226–4233.

Holms H. Flux analysis and control of the central metabolic pathways in *Escherichia coli*. FEMS Microbiol Rev. 1996; 19(2):85–116.

Hui S, Silverman JM, Chen SS, Erickson DW, Basan M, Wang J, Hwa T, Williamson JR. Quantitative proteomic analysis reveals a simple strategy of global resource allocation in bacteria. Mol Syst Biol. 2015; 11(1):784.

Keren L, Hausser J, Lotan-Pompan M, Slutskin IV, Alisar H, Kaminski S, Weinberger A, Alon U, Milo R, Segal E. Massively parallel interrogation of the effects of gene expression levels on fitness. Cell. 2016; 166(5):1282–1294.

Klumpp S, Zhang Z, Hwa T. Growth-rate dependent global effects on gene expression in bacteria. Cell. 2009 dec; 139(7):1366.

Kochanowski K, Gerosa L, Brunner SF, Christodoulou D, Nikolaev YV, Sauer U. Few regulatory metabolites coordinate expression of central metabolic genes in *Escherichia coli*. Mol Syst Biol. 2017 jan; 13(1).

Kussell E, Leibler S. Phenotypic diversity, population growth, and information in fluctuating environments. Science (80-). 2005; 309(5743):2075–2078.

Maarleveld TR, Wortel MT, Olivier BG, Teusink B, Bruggeman FJ. Interplay between Constraints, Objectives, and Optimality for Genome-Scale Stoichiometric Models. PLoS Comput Biol. 2015; 11(4):1–21.

Molenaar D, van Berlo R, de Ridder D, Teusink B. Shifts in growth strategies reflect tradeoffs in cellular economics. Mol Syst Biol. 2009; 5(323):323.

Monod J. The Growth of Bacterial Cultures. Annu Rev Microbiol. 1949 oct; 3(1):371–394.

Mori M, Hwa T, Martin OC, De Martino A, Marinari E. Constrained allocation Flux Balance Analysis. PLoS Comput Biol. 2016; 12(6):1–24.

Müller S, Regensburger G, Steuer R. Enzyme allocation problems in kinetic metabolic networks: Optimal solutions are elementary flux modes. J Theor Biol. 2014; 347(1):182–190.

Nanchen A, Schicker A, Sauer U. Nonlinear dependency of intracellular fluxes on growth rate in miniaturized continuous cultures of *Escherichia coli*. Appl Environ Microbiol. 2006; 72(2):1164–1172.

Nilsson A, Nielsen J. Metabolic Trade-offs in Yeast are Caused by F1F0-ATP synthase. Sci Rep. 2016; 6(November 2015):22264.

O'Brien EJ, Lerman JA, Chang RL, Hyduke DR, Palsson BO. Genome-scale models of metabolism and gene expression extend and refine growth phenotype prediction. Mol Syst Biol. 2014; 9(1):693–693.

Peebo K, Valgepea K, Maser A, Nahku R, Adamberg K, Vilu R. Proteome reallocation in *Escherichia coli* with increasing specific growth rate. Mol Biosyst. 2015; 11:1184–1193.

Planque R, Hulshof J, Teusink B, Hendriks J, Bruggeman FJ. Maintaining maximal metabolic flux by gene expression control. bioRxiv. 2017; .

Postma E, Verduyn C, Scheffers WA, Van Dijken JP. Enzymic Analysis of the Crabtree Effect in Glucose-Limited Chemostat Cultures of Saccharomyces-Cerevisiae. Appl Environ Microbiol. 1989; 55(2):468–477.

Price ND, Reed JL, Palsson BØ. Genome-scale models of microbial cells: evaluating the consequences of constraints. Nat Rev Microbiol. 2004; 2(11):886–897.

Sæther BE, Engen S. The concept of fitness in fluctuating environments. Trends Ecol & Evol. 2015; 30(5):273–281.

Sánchez BJ, Zhang C, Nilsson A, Lahtvee PJ, Kerkhoven EJ, Nielsen J. Improving the phenotype predictions of a yeast genome scale metabolic model by incorporating enzymatic constraints. Mol Syst Biol. 2017 aug; 13(8).

Schuster S, Fell DA, Dandekar T. A general definition of metabolic pathways useful for systematic organization and analysis of complex metabolic networks. Nat Biotechnol. 2000; 18(3):326–332.

Scott M, Gunderson CW, Mateescu EM, Zhang Z, Hwa T. Interdependence of cell growth and gene expression: origins and consequences. Science (80-). 2010; 330(6007):1099–1102.

Scott M, Klumpp S, Mateescu EM, Hwa T. Emergence of robust growth laws from optimal regulation of ribosome synthesis. Mol Syst Biol. 2014; 10(8):747.

Smith JM. Optimization theory in evolution. Annu Rev Ecol Syst. 1978; 9(1):31–56.

Smith RF, Humphreys S, Hockaday TDR. The measurement of plasma acetate by a manual or automated technique in diabetic and non-diabetic subjects. Ann Clin Biochem. 1986; 23(3):285–291.

Snoep JL, Mrwebi M, Schuurmans JM, Rohwer JM, Teixeira de Mattor MJT. Control of specific growth rate in *Saccharomyces cerevisiae*. Microbiology. 2009; 155(5):1699–1707.

von Stosch M, Rodrigues de Azevedo C, Luis M, Feyo de Azevedo S, Oliveira R. A principal components method constrained by elementary flux modes: analysis of flux data sets. BMC Bioinformatics. 2016; 17(1):200.

Szenk M, Dill KA, de Graff AMR. Why do fast-growing bacteria enter overflow metabolism? Testing the membrane real estate hypothesis. Cell Syst. 2018 apr; 5(2):95–104.

Tännler S, Decasper S, Sauer U. Maintenance metabolism and carbon fluxes in Bacillus species. Microb Cell Fact. 2008; 7(1):19.

Terzer M, Stelling J. Large-scale computation of elementary flux modes with bit pattern trees. Bioinformatics. 2008; 24(19):2229–2235.

Vazquez A, Beg QK, DeMenezes MA, Ernst J, Bar-Joseph Z, Barabási AL, Boros LG, Oltvai ZN. Impact of the solvent capacity constraint on *E. coli* metabolism. BMC Syst Biol. 2008 jan; 2:7.

Vazquez A, Oltvai ZN. Macromolecular crowding explains overflow metabolism in cells. Sci Rep. 2016; 6:31007.

Weiße AY, Oyarzún DA, Danos V, Swain PS. Mechanistic links between cellular trade-offs, gene expression, and growth. Proc Natl Acad Sci. 2015; 112(9):E1038—-E1047.

Wortel MT, Peters H, Hulshof J, Teusink B, Bruggeman FJ. Metabolic states with maximal specific rate carry flux through an elementary flux mode. FEBS J. 2014; 281(6):1547–1555.

Zhuang K, Vemuri GN, Mahadevan R. Economics of membrane occupancy and respiro-fermentation. Mol Syst Biol. 2011; 7(500):500.

Appendix 1

Elementary Flux Modes as the building blocks of metabolism

The structure of a metabolic network can be denoted by its stoichiometric matrix $\boldsymbol{N}$. Each column of this matrix denotes which metabolites are used (negative entries) and produced (positive entries) in one reaction. In a metabolic network with m metabolites and r reactions this results in an $m \times r$-matrix. A steady-state flux vector $\boldsymbol{v} \in \mathbb{R}^r$ must then be in the nullspace of this matrix $\boldsymbol{N} \cdot \boldsymbol{v} = 0$. Some reactions are reversible, but others are modelled as irreversible, $v_j \geq 0$. This causes the feasible flux vectors to form a polyhedron $\mathcal{P}$ (rather than a linear subspace) in so-called flux space (**?**).

For a flux vector, $\boldsymbol{v} \in \mathbb{R}^r$, its 'support' is the set of participating reactions $R(\boldsymbol{v}) = \{j : v_j \neq 0\}$. An elementary flux mode $\mathbf{EFM} = (V_1, \ldots V_r)^T \in \mathcal{P}$ minimizes the number of elements in $R(\mathbf{EFM})$. In other words, if there is a $\boldsymbol{v}' \in \mathcal{P}$ such that $R(\boldsymbol{v}') \subseteq R(\mathbf{EFM})$ then we must have $\mathbf{EFM} = \alpha \boldsymbol{v}'$ for some $\alpha \neq 0$. Another way of phrasing this is that none of the used reactions can be set to zero in the EFM without violating the steady state condition.

EFMs are defined up to a constant: if $\boldsymbol{v}$ is an EFM, than so is $\alpha \boldsymbol{v}$ for any $\alpha \in \mathbb{R}$. This has two important consequences. First, the ratio between flux entries in an EFM are fixed, and second, we may scale one entry of an EFM to 1. We will always choose the last element of an **EFM** to be 1, and will denote the ith EFM by $\mathbf{EFM}^i = (V_1^i, \ldots, V_{r-1}^i, 1)^T \in \mathbb{R}^r$, with all V_j^i uniquely determined by stoichiometry.

Gagneur and Klamt showed that in any metabolic network, these EFMs coincide with the extreme rays of the pointed polyhedral cone $\mathcal{P}$ (**?**). This implies that in a metabolic network every steady state flux vector $\boldsymbol{v}$ can be written as a unique conical combination of the EFMs (**?**):

$$\boldsymbol{v} = \lambda_1 \mathbf{EFM}^1 + \ldots + \lambda_F \mathbf{EFM}^F, \text{ where } \lambda_i \geq 0, \tag{1}$$

where the multiplication factors λ_i denote how much the ith EFM is used and F denotes the total number of EFMs in the network. Note that, although the Elementary Flux Modes are constant vectors defined by stoichiometry, the λ_i-factors are variable and dependent on metabolite concentrations. We will make this dependence more precise in ***Appendix 5***. Equation (1) shows that EFMs are the basic building blocks of steady state metabolism.

We will consider optimisation of some objective flux v_r at steady state. Therefore, we only need to consider those EFMs which have a nonzero r^{th} flux value. Without loss of generality, we can make this the last entry in the vector, and will scale the objective flux to 1 throughout the SI. The interpretation of the λ_i factors in (1) may now be reinterpreted as the fraction of $\mathbf{EFM}^i$ contributing to one unit of objective flux.

Individual metabolic reactions in the network are assumed to be catalyzed by enzymes, and reaction rates generally are well described by $v_j = e_j f_j(\boldsymbol{x})$, where e_j denotes the concentration of enzyme j, and $f_j(\boldsymbol{x})$ denotes the reaction kinetics (***Cornish-Bowden***, 2014). We will assume this type of dependence throughout the SI, and assume that each enzyme catalyzes one reaction. In some situations, we will distinguish between external concentrations $\boldsymbol{x}^E$ (which are assumed to be parameters), and internal concentrations $\boldsymbol{x}^I$ (which may be varied, for instance to obtain a maximal objective flux).

Appendix 2

Elementary Flux Modes as the building blocks of optimal metabolism

We here prove the main result of this study, the extremum principle. Let us consider a metabolic network characterized by stoichiometry matrix $\boldsymbol{N}$. We ask which vector $\boldsymbol{v}$ in the steady state flux cone $\mathcal{P}$ maximizes a given objective flux v_r under a given set of K enzymatic constraints.

Theorem 1. *Consider a metabolic network characterized by $\boldsymbol{N}$. Let v_r be an objective flux v_r to be maximized at steady state, under K linear enzymatic constraints of the form:*

$$C_k^{\Sigma} := \sum_{j=1}^{r} C_k^j e_j \leq 1 \qquad \text{for } k \in \{1, \dots, K\}.$$

Then, at most K Elementary Flux Modes are used in the optimal solution.

Proof. We may assume that $v_j \geq 0$ for all reactions in the network by splitting all reversible reactions into a forward and a backward reaction (**?**).

According to Equation (1), the optimal solution can always be expressed as a conical combination of EFMs. We may delete all EFMs that have a zero r^{th} component, because these EFMs will only bring costs and no extra objective flux. As discussed in ***Appendix 1***, we rescale every EFM such that it is a vector of the form $\mathbf{EFM}^i = (V_1^i, \dots, V_{r-1}^i, 1)^T \in \mathbb{R}^r$. The objective flux for a flux vector $\boldsymbol{v}$ can now be written as

$$v_r = \left(\lambda_1 \mathbf{EFM}^1 + \dots + \lambda_M \mathbf{EFM}^M\right)_r = \lambda_1 + \lambda_2 + \dots + \lambda_M, \text{ where } \lambda_i \geq 0, \tag{2}$$

where M is the number of EFMs containing a nonzero v_r. Since the EFMs are fixed vectors, we may only choose appropriate λ_i. Since $v_j = \sum_{i=1}^{M} \lambda_i V_j^i = e_j f_j(\boldsymbol{x})$, we have

$$e_j = \sum_{i=1}^{M} \lambda_i \frac{V_j^i}{f_j(\boldsymbol{x})}.$$

This allows us to rewrite enzyme constraint C_k^{Σ} as

$$\begin{aligned} C_k^{\Sigma} &= \sum_{j=1}^{r} C_k^j e_j \\ &= \sum_{j=1}^{r} C_k^j \sum_{i=1}^{M} \lambda_i \frac{V_j^i}{f_j(\boldsymbol{x})} \\ &= \sum_{i=1}^{M} \lambda_i \sum_{j=1}^{M} C_k^j \frac{V_j^i}{f_j(\boldsymbol{x})} \\ &=: \sum_{i=1}^{M} \lambda_i d_k^i(\boldsymbol{x}). \end{aligned}$$

The *cost vector* $\boldsymbol{d}^i(\boldsymbol{x})$ for the ith EFM, the components of which are given by

$$d_k^i(\boldsymbol{x}) = \sum_{j=1}^{M} C_k^j \frac{V_j^i}{f_j(\boldsymbol{x})}. \tag{3}$$

plays a central role in the whole paper.

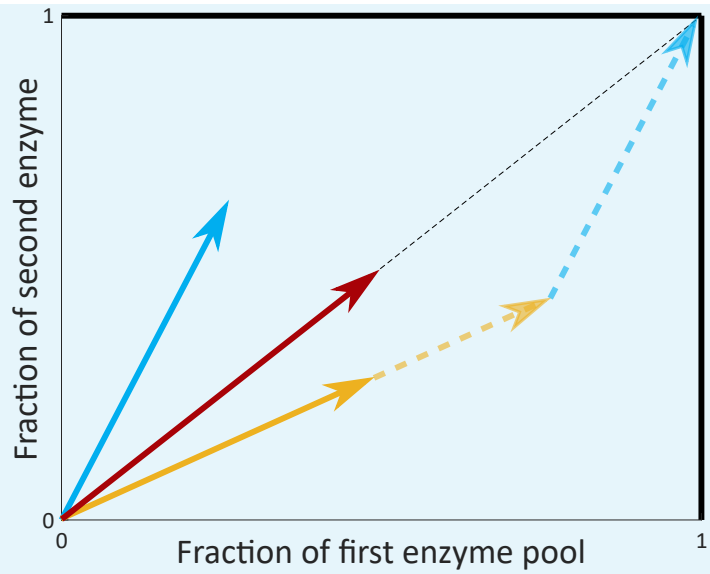

Appendix 2 Figure 1. Cost vectors in the space of constraints. A cost vector denotes the fractions of the two limited enzyme pools that are needed to produce one unit of objective flux through this EFM. The objective flux is optimized by taking a sum of multiples $\lambda_1 \boldsymbol{d}^1 + \cdots + \lambda_m \boldsymbol{d}^M$ without leaving the box of constraints and while maximizing the sum of these multiples $\lambda_1 + \cdots + \lambda_m$. The optimal use of the EFMs is here indicated by the dashed lines.

The vector denotes the cost for the enzymes in constraint k (the k-*enzymes*) to obtain one unit of flux through **EFM**^{i} (and therefore also the enzymatic cost to increase this flux by some factor). We can now rewrite the optimization problem in the statement of the theorem. Recalling the division between external and internal metabolic concentrations, $\boldsymbol{x}^E$ and $\boldsymbol{x}^I$ resp., we now need to solve

$$\max_{\boldsymbol{x}^I, \lambda} \left\{ \sum \lambda_i \mid \lambda_i \geq 0,\ \boldsymbol{D}(\boldsymbol{x}) \cdot \lambda \leq \mathbf{1} \right\}, \tag{4}$$

where $\boldsymbol{D} = \begin{bmatrix} \boldsymbol{d}^1(\boldsymbol{x}) & \cdots & \boldsymbol{d}^r(\boldsymbol{x}) \end{bmatrix}$ is the cost vector matrix. The relation $\boldsymbol{D}(\boldsymbol{x}) \cdot \lambda \leq 1$ shows that the optimal λ vector indeed depends on the metabolite concentrations $\boldsymbol{x}$, as was indicated below equation (1).

Following[a] Wortel et al. (***Wortel et al.***, 2014), we now use a subtle mathematical argument. We fix $\boldsymbol{x} = \boldsymbol{x}_0$, so that the enzyme saturations $f_j(\boldsymbol{x}_0)$ are constant. This will give us a fixed cost vector for each EFM. The remaining optimization problem is then visualized in ***Figure 1***, where cost vectors of some EFMs are plotted in a box of constraints. Finding the optimal solution is now equivalent to finding a sum of scalar multiples of the cost vectors without leaving the box of constraints while maximizing the sum of these multiplicities. The example in ***Figure 1*** shows only 2 constraints, but in general we would of course have M vectors in a K-dimensional cube.

In the general case, we can first get an intuition of why M constraints lead to the usage of at most M EFMs since all M linearly-independent vectors form a basis of an M-dimensional space. We can thus always take a combination of M vectors to reach the point where all constraints are met with equality. However, we should still be careful because we could end up with negative λ's for some of the EFMs. We continue with the proof by rewriting the problem in a Linear Programming (LP) form. [

em]2em Maximize $v_r = \mathbf{1} \cdot \lambda$,
subject to
$\boldsymbol{A}\lambda \leq \boldsymbol{z}$,
where

$$\boldsymbol{A} = \begin{pmatrix} -\mathbb{I}_{M\times M} \\ \boldsymbol{D} \end{pmatrix}, \quad \boldsymbol{z} = \begin{pmatrix} \mathbf{0}_{M\times 1} \\ \mathbf{1}_{K\times 1} \end{pmatrix}.$$

The solutions for this problem are vectors $\lambda \in \mathbb{R}^M$. The solution space of this linear program is an M-dimensional polytope, bounded by the hypersurfaces given by the constraints. The most important theorem of LP teaches us that an optimal solution is found among the vertices of this polytope. The dimension of such vertices is zero, which means that optimal solutions satisfy at least M of the $K+M$ constraints with equality. Therefore at most $(K+M)-M = K$ constraints can be satisfied with strict inequality. These K inequalities could be concentrated in the $\lambda_i \geq 0$ part, which means that the corresponding K elementary flux modes are used. Thus, an optimal solution can use no more EFMs than there are active constraints in the system, thereby proving the theorem for any arbitrary vector of metabolite concentrations $\boldsymbol{x}$.

Finally, since the theorem is true for any set of metabolite concentrations $\boldsymbol{x}$, it of course also true for a vector of concentrations $\boldsymbol{x}_{\text{opt}}$ that optimizes the objective flux under K enzymatic constraints over all possible metabolite concentration vectors. (More precisely, $\boldsymbol{x}^I$ may be chosen optimally for any given $\boldsymbol{x}^E$.) Finally, we note that the choice of EFMs in the optimal solution depends on the concentration vector $\boldsymbol{x}$; as $\boldsymbol{x}_{\text{opt}}$ is unknown, the choice of EFMs in the real optimum does not follow directly from the theorem. □

The theorem that maximal specific flux is attained in an EFM (***Wortel et al.***, 2014; ***Müller et al.***, 2014) is a special case of Theorem 1. In the cost vector formalism as introduced in the proof of Theorem 1, it is visualized by cost vectors on a line rather than in a box, because there is only one enzymatic constraint (total enzyme concentration is bounded). In this case, there is indeed a shortest cost vector for all but a negligible subset of situations. (When multiple vectors are equally short, then all of these are equally good optimal solutions.)

The following corollary can be used to find out how many constraints are active when we observe a certain number of active EFMs. It is the contrapositive of Theorem 1 and therefore mathematically equivalent. The reason that it is stated separately is the difference in biological applicability: the theorem is a predictive statement while the corollary is descriptive.

Corollary 2. *If a flux v_r is optimized and M elementary flux modes are used, then at least M linear enzymatic constraints must be active.*

[a] Note that in the proof of Wortel et al. the vector of metabolite concentrations $\boldsymbol{x}$ was fixed to its optimal value $\boldsymbol{x}_{\text{opt}}$ before proceeding. This is not possible, since the optimal value is dependent on the choice of enzyme concentrations and these have yet to be determined. The correct argument is proving the theorem for all fixed $\boldsymbol{x}$, and therewith for the optimal $\boldsymbol{x}$.

Appendix 3

The generality of enzyme constraints

Recall that we model growth optimisation as the maximisation of the cell synthesis flux (v_r). We assume that all reactions are catalyzed by an enzyme and that the reaction rate is proportional to the enzyme concentration, i.e. $v_i = e_i f_i(\boldsymbol{x})$. Let us now pick a certain steady state flux distribution that leads to cell growth: $(v_1, \dots, v_r)$. If the growth rate is limited, this means that there is a maximal value for v_r. However, without enzyme-concentration constraints, we could always increase the flux by adding enzymes in the right proportions: $(\frac{v_1}{f_1(\boldsymbol{x})}, \dots, \frac{v_r}{f_r(\boldsymbol{x})})$. The fact that the growth rate is not infinite therefore either shows that enzyme constraints must be active, or that we are in some limit where $v_i = e_i f_i(\boldsymbol{x})$ is no longer true. This last possibility cannot be excluded, but we expect the enzyme constraints to have a more dominant effect.

Other growth-limiting constraints that have been studied, such as a limited solvent capacity of the (mitochondrial) membrane or the cytosol can generally be viewed as protein-concentration constraints. A limited membrane area results in a constrained pool of membrane proteins:

$$\sum_{i|e_i=\text{membrane}} w_i e_i \leq C,$$

where w_i is the needed membrane area for one mol of the ith membrane protein and C is the membrane area per cell volume.

Cytosolic volume can be written as

$$\sum_{i|e_i=\text{cytosol}} w_i e_i \leq C,$$

where w_i is now the needed cytosolic volume for one mol e_i and C is the cytosolic volume per cell volume.

Appendix 4

Most models of mixed behaviour are instances of the extremum principle

We here divide the existing models into the following classes:

1. **Genome-scale, classical FBA-models with only fluxes as variables and flux constraints.** These models omit enzyme kinetics and metabolite concentrations. When all reversible reactions are split into two irreversible reactions (as we have done before, ***Appendix 2***), the steady-state assumption leads to a flux cone. This cone has extreme rays which are the Elementary Flux Modes of the metabolic network (***Gagneur and Klamt***, 2004). Under one flux constraint, this cone can become a bounded polyhedron. It follows from linear programming that an objective, which in this context is a weighted sum of fluxes, will be maximised in a vertex of the polyhedron, i.e. the flux is maximised in an EFM (***Wortel et al.***, 2014). The addition of a new constraint will intersect the polyhedron to create a new polyhedron, with a new set of vertices. This set will contain some of the old vertices, as well as new vertices which are convex combinations of the old vertices. These new vertices are thus convex combinations of two EFMs. If the objective flux is maximal in such a new vertex, then two constraints are active. If however, the objective is optimised in an old vertex, then only one constraint is active and one EFM will be used. In any case, the number of active EFMs is bounded by the number of active constraints.
2. **Genome-scale and coarse-grained FBA-models with fluxes as variables and enzyme-concentration constraints (*van Hoek and Merks*, 2012; *Basan et al.*, 2015; *Vazquez and Oltvai*, 2016; *Nilsson and Nielsen*, 2016).** The enzyme-concentration constraints can, at fixed metabolite concentrations and the assumption that $v_i = e_i f_i(\boldsymbol{x})$ be transformed into linear flux constraints. Then we can treat this class of models similar to the models in class 1.
3. **Coarse-grained kinetic models (*Weiße et al.*, 2015; *Molenaar et al.*, 2009).** These models obey the extremum principle, provided that, when we set the metabolite concentrations to their optimal values, the resulting optimisation problem (either in flux or enzyme space) is a linear program.
4. **ME-models with enzyme concentrations as variables and enzyme-concentration constraints.** Strictly speaking, ME-models do not fall under the class of models that obey the extremum principle. However, a similar principle exists for flux modes associated with ME-models, an unpublished finding by ourselves.

•

Appendix 5

'Unfixing' the metabolite concentrations

Fixing the metabolite concentrations to an arbitrary $\boldsymbol{x_0}$ is a subtle step in the proof, since the outcome of the optimisation procedure depends on the choice of $\boldsymbol{x_0}$. Because of the fixed concentrations, the only quantities that influence the cell's metabolism are the enzyme concentrations. These can then be easily optimized. Although considering fixed concentrations helps in the proof, in biological applications we would often like to know how changing a specific external concentration influences a cell's optimal choice. For example, in a yeast cell growing on glucose we know that the cell has different strategies corresponding to different external glucose concentrations. It will use the efficient respiration strategy at low glucose levels, while it uses a combination of respiration and fermentation at higher levels.

As was argued in the proof of Theorem 1, we may rewrite the optimisation problem so that the $\boldsymbol{x}$-dependence is restricted to the cost vectors

$$d_k^i(\boldsymbol{x}) = \sum_{j=1}^{r} C_k^j \frac{V_j^i}{f_j(\boldsymbol{x})}.$$

This means that the general picture will always be as in ***Figure 1***, but that the cost vectors can be adjusted by the metabolite concentrations $\boldsymbol{x}$, see the shaded areas in ***Figure 1***. It is important to note that $\boldsymbol{x}$ consists of the concentrations of all metabolites that affect the metabolism in the network. As mentioned before, these can be divided into two groups: an external metabolite group $\boldsymbol{x^E}$ which can not be controlled by the cell and an internal metabolite group $\boldsymbol{x^I}$ which can be adjusted. The external concentrations are part of the optimization problem, while $\boldsymbol{x^I}$ is part of the solution.

Using the cost vector formalism, we can provide some insight into how the metabolite concentrations affect the arrows. Recall that maximizing the objective flux is equivalent to fitting the largest sum of multiples of cost vectors in the box of constraints. An important point to note is that a solution using K elementary flux modes in the case of K constraints is not as probable as one might suspect. There are two reasons for this.

First, internal metabolite concentrations $\boldsymbol{x^I}$ may be adjusted to use one EFM which satisfies more than one constraint simultaneously. In ***Figure 1*** this means that the cost vector of one EFM is pointed exactly diagonally, such as the red arrow. In the overflow metabolism examples, the diagonal arrow is the respiration cost vector. To what extent cost vectors can be adjusted by internal concentrations to become diagonal is largely dependent on the enzyme kinetics of the network.

Second, it could be suboptimal or not feasible to satisfy some constraint with equality. In this case there are $K-1$ active constraints and a maximum of $K-1$ Elementary Flux Modes will thus be chosen for any internal metabolite concentration. A cell will only start using an extra EFM when this new EFM can provide more flux by hitting the currently inactive constraint. This means that the enzyme usage of the currently active constraints per unit flux must be lower for the new EFM than for the current combination of EFMs. Otherwise, it is better not to hit the last constraint at all and keep using the $K-1$ EFMs.

What should be clear from the above discussion is that a mixed strategy is a very special situation in metabolism. The observation of a mixed strategy therefore provides much information about the number of constraints that act on the system. In the case of 2 EFMs we can summarize this in the following conditions, which we prove to be necessary and sufficient in Theorem 6. The conditions are illustrated in ***Figure 1***.

A cell that optimizes an objective flux uses a mixture of EFMs if and only if
1) there are at least two enzymatic constraints,
2) EFMs with off-diagonal cost vectors exist in the direction of both constraints,
3) each constraint has a different EFM that uses the smallest fraction of the corresponding enzyme pool,
4) it is not feasible to hit both constraints with a diagonal EFM for which the cost vector is in the triangle spanned by the two cost vectors.

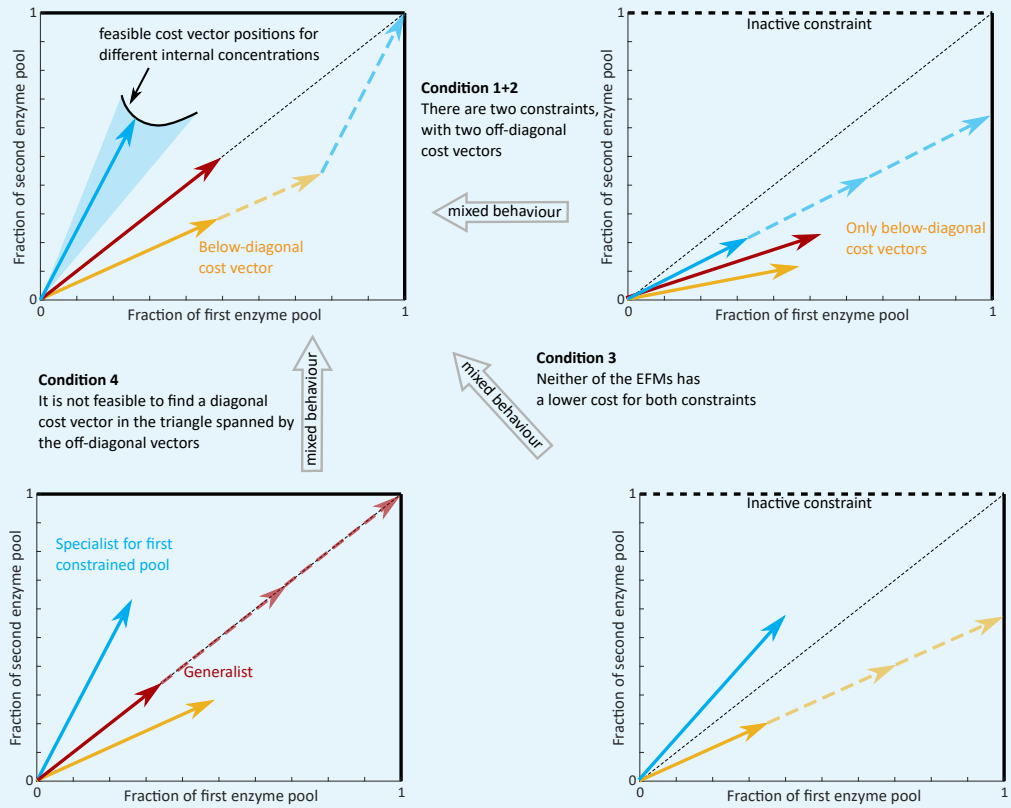

Appendix 5 Figure 1. We distinguish four necessary and sufficient conditions for a mixture of EFMs to be optimal. The black line and blue shaded region in the left upper plot indicates the feasible cost vector positions at different internal concentrations. These positions were left out for the other cost vectors for simplicity, only the optimal cost vectors are shown there.

Before we prove this in a theorem we need some preparation in the form of a definition and two lemmas.

Definition 1. *Let two cost vectors $\boldsymbol{d}^1$ and $\boldsymbol{d}^2$ satisfy $d_1^1 \leq d_2^1$, and $d_1^2 \geq d_2^2$. They are said to be in a* mixable position *if $d_1^1 > d_1^2$ and $d_2^1 < d_2^1$.*

In many of the results that follow, the optimisation problem as phrased in the previous theorem, but now involving only two cost vectors, will be studied. For future reference, we state it here in full,

$$\max_{\boldsymbol{x}^I, \lambda} \left\{ \sum \lambda_i \mid \lambda_i \geq 0,\ \boldsymbol{D}(\boldsymbol{x}) \cdot \lambda \leq \mathbf{1} \right\}, \tag{5}$$

where $\boldsymbol{D} = \left[\boldsymbol{d}^1(\boldsymbol{x}), \boldsymbol{d}^2(\boldsymbol{x})\right]$ is the cost vector matrix.

Lemma 3. *Consider two cost vectors $\boldsymbol{d}^1(\boldsymbol{x})$, $\boldsymbol{d}^2(\boldsymbol{x})$ in mixable position, and consider Problem* (5)*. Then the optimal solution will satisfy $\boldsymbol{D} \cdot \lambda = [1, 1]^\intercal$.*

Proof. Let us say, for a contradiction that this is not true. Assume without loss of generality that $\boldsymbol{D} \cdot \lambda^{\text{opt}} = [1, 1-c]^\intercal$. But then there is only one active constraint so only one EFM will be used in the optimal solution, let us say $\lambda_1^{\text{opt}} \boldsymbol{d}^1 = [1, 1-c]^\intercal$. This means that $d_1^1 > d_2^1$ and since the vectors are in mixable position we know that $d_1^2 \leq d_2^2, d_1^2 < d_1^1, d_2^2 > d_2^1$.

We can now find a better solution by combining the cost vectors. Choose $\epsilon = \frac{c}{2(d_2^2 - d_2^1)}$. Then consider the combination $(\lambda_1^{\text{opt}} - \epsilon)\boldsymbol{d}^1 + \epsilon \boldsymbol{d}^2$. We have

$$(\lambda_1^{\text{opt}} - \epsilon) d_1^1 + \epsilon d_1^2 = 1 - \frac{c}{2(d_2^2 - d_2^1)} d_1^1 + \frac{c}{2(d_2^2 - d_2^1)} d_1^2 = 1 - \frac{c(d_1^1 - d_1^2)}{2(d_2^2 - d_2^1)} < 1,$$

$$(\lambda_1^{\text{opt}} - \epsilon) d_2^1 + \epsilon d_2^2 = 1 - c - \frac{c}{2(d_2^2 - d_2^1)} d_2^1 + \frac{c}{2(d_2^2 - d_2^1)} d_2^2 = 1 - c + \frac{c(d_2^2 - d_2^1)}{2(d_2^2 - d_2^1)} = 1 - \frac{c}{2} < 1.$$

We thus hit none of the constraints while we obtain the same objective value $(\lambda_1^{\text{opt}} - \epsilon) + \epsilon = \lambda_1^{\text{opt}}$. Therefore we can increase either λ_1 or λ_2 which will give a higher objective value, in contradiction with the assumption that λ_1^{opt} was the maximum. □

Lemma 4. *Consider Problem* (5)*, and choose metabolite concentrations* $\boldsymbol{x}$*. Assume that* $\boldsymbol{d}^1(\boldsymbol{x}), \boldsymbol{d}^2(\boldsymbol{x})$ *are in mixable position. Then we have* $\lambda_1^{opt}(\boldsymbol{x}) + \lambda_2^{opt}(\boldsymbol{x}) = \frac{1}{\beta}$*, where* β *is the intersection of the convex combination of the cost vectors and the diagonal of the constraint box, i.e.*

$$\beta \begin{bmatrix} 1 \\ 1 \end{bmatrix} = t \begin{bmatrix} d_1^1(\boldsymbol{x}) \\ d_2^1(\boldsymbol{x}) \end{bmatrix} + (1-t) \begin{bmatrix} d_1^2(\boldsymbol{x}) \\ d_2^2(\boldsymbol{x}) \end{bmatrix} \quad \textit{for suitable } t, \beta. \tag{6}$$

Proof. We suppress the dependence on $\boldsymbol{x}$ in the notation, as $\boldsymbol{x}$ is fixed throughout. Because the vectors are in mixable position, $\boldsymbol{D}$ is invertible, and Lemma 3 tells us that the optimal λ for these metabolite concentrations satisfies $\boldsymbol{D} \cdot \lambda^{\text{opt}} = [\boldsymbol{d}^1, \boldsymbol{d}^2] \cdot \lambda^{\text{opt}} = [1, 1]^\intercal$. Let t and β be chosen such that the convex combination of $\boldsymbol{d}^1$ and $\boldsymbol{d}^2$ lies on the diagonal, i.e., $t\boldsymbol{d}^1 + (1-t)\boldsymbol{d}^2 = \beta \mathbf{1}$. Then

$$\boldsymbol{D} \cdot \begin{bmatrix} t \\ 1-t \end{bmatrix} = \beta \mathbf{1}, \qquad \Longleftrightarrow \qquad \boldsymbol{D} \cdot \begin{bmatrix} \frac{t}{\beta} \\ \frac{1-t}{\beta} \end{bmatrix} = \mathbf{1}.$$

But also $\boldsymbol{D} \cdot \lambda^{\text{opt}} = \mathbf{1}$, and we conclude

$$\lambda^{\text{opt}} = \begin{bmatrix} \frac{t}{\beta} \\ \frac{1-t}{\beta} \end{bmatrix},$$

and

$$\lambda_1^{\text{opt}} + \lambda_2^{\text{opt}} = \frac{1}{\beta}.$$

□

This Lemma gives a very useful way to compare different pairs of EFMs in the constraint box. For each pair in mixable position, we determine the point where the convex combination of the pair intersects the diagonal. The pair of vectors whose intersection point lies closest to the origin has highest sum of λ's, and gives rise to the highest flux.

Corollary 5. *A diagonal cost vector will give rise to a higher objective flux than a combination of two off-diagonal cost vectors if and only if the diagonal cost vector is contained in the triangle spanned by the off-diagonal vectors.*

Theorem 6. *Consider Problem* (5) *for any number of cost vectors. The global maximum will have at least two nonzero* λ*'s, say* $\lambda_1, \lambda_2 > 0$*, if and only if*

1. *there are at least two linear enzymatic constraints, i.e.* $\sum_{j=1}^{r} C_1^j e_j \leq 1$ *and* $\sum_{j=1}^{r} C_2^j e_j \leq 1$*, where the vectors* $\boldsymbol{C}_1$ *and* $\boldsymbol{C}_2$ *are linearly independent,*
2. *corresponding to each constraint there is an off-diagonal cost vector, i.e.* $d_1^i < d_2^i$ *and* $d_1^j > d_2^j$*,*
3. *each constraint has a different EFM with the smallest component in the direction of that constraint, i.e.* $d_1^i < d_1^j$ *and* $d_2^i > d_2^j$*,*
4. *we can not find an EFM with a diagonal cost vector* $\boldsymbol{d}^p$ *such that* $\boldsymbol{d}^p = \lambda_i d^i + \lambda_j d^j$*, with* $\lambda_i + \lambda_j \leq 1$*.*

Proof. We can prove the 'only if' part of this theorem by its contrapositive. Let us for each condition assume that it is not satisfied and show that this will result in the usage of fewer than 2 EFMs.

1. If there are no two constraints, Theorem 1 tells us that at most one EFM will be used, so only one λ will be nonzero.
2. A combination of two EFMs will give a total objective flux of $\lambda_i + \lambda_j$, while it should satisfy $\lambda_i d_1^i + \lambda_j d_1^j \leq 1$ and $\lambda_i d_2^i + \lambda_j d_2^j \leq 1$. Let us say, without loss of generality, that there is no off-diagonal cost vector for the first constraint, which means that for all EFMs we have $d_1^i \geq d_2^i$. If both vectors are diagonal, the global maximum will only use the shortest vector (except for the negligible situation in which both diagonal vectors have the same length). So, let us assume that one of the vectors is off-diagonal $d_1^i < d_2^i$, because two diagonal vectors will never partake in a mixture of EFMs. Then the second constrained pool will never be fully used, since

$$\lambda_i d_2^i + \lambda_j d_2^j < \lambda_i d_1^i + \lambda_j d_1^j \leq 1.$$

   But then there is in fact only one active constraint and Theorem 1 thus tells us that only one EFM will be used.
3. Let us say, without loss of generality, that **EFM**^{i} has the off-diagonal cost vector for constraint 1 and **EFM**^{j} for constraint 2. By definition $d_1^i < d_2^i$ and $d_2^j < d_1^j$, but to contradict the condition we also have $d_1^j \leq d_1^i$, which implies $d_2^j < d_2^i$ too, then

$$(\lambda_i + \lambda_j) d_k^i < \lambda_i d_k^i + \lambda_j d_k^j \leq 1$$

   for both constraints. The feasible flux by using only **EFM**^{i} can therefore be larger than $\lambda_i + \lambda_j$ and only λ_i will be greater than zero in the optimum.
4. If there was a diagonal cost vector in the triangle spanned by the off-diagonal cost vectors then the corresponding EFM would give rise to a higher flux than the combination of the off-diagonals by Lemma 4.

The 'if'-part of the theory remains. Assume for a contradiction that a pure EFM, **EFM**^{p} is used in the optimal solution. We know that there are two constraints, so this EFM could either hit both of these constraints or only hit one. In the first case, this EFM has a diagonal cost vector, but by conditions 2 and 4 there are then also two off-diagonal cost vectors that span a triangle which does not contain the diagonal cost vector. By Lemma 4, we know that this combination could then produce a higher flux than the pure EFM. In the case that the EFM hits only one constraint, say the first, the EFM has an off-diagonal cost vector, i.e. $d_1^p > d_2^p$. Pure usage of this EFM will not hit the second constraint, $\lambda_p d_2^p < 1$. Conditions 2 and 3 imply that there is another EFM, **EFM**^{i} in mixable position with **EFM**^{p}. Pure usage of this i^{th} EFM will not hit the first constraint, but Lemma 3 states that the maximum with these cost vectors will hit both constraints. Therefore, the maximum must have $\lambda_i, \lambda_p > 0$. This completes the proof. □

Appendix 6

The effect of tightening the constraints

An experimental perturbation can often be explained as affecting the constrained enzyme pools. Either one of the constrained enzyme pools is tightened, or the cost with respect to one of the enzyme pools for an EFM to make one unit flux is increased. These two types of perturbations are mathematically equivalent, so that from now on we will focus on the tightening of constraints. The situation in which the costs for one EFM is increased more than the cost for the other EFM will be discussed in ***Appendix 7***. Here we show how different perturbations affect the gradual transition from usage of one EFM to a combination of two EFMs (as in overflow metabolism).

First we define the exact point of transition between one and two EFMs in the optimum.

Definition 2. *Consider Problem* (5) *and call the optimal flux solutions at certain environmental conditions* $\lambda^{opt}(\boldsymbol{x}^E)$*. The* critical conditions *are external environmental conditions* $\boldsymbol{x}^E_{cr} \in \mathbb{R}^e$*, for which there is a continuous map* $p(\tau) : [-1, 1] \to \mathbb{R}^e$ *with* $p(0) = x^E_{cr}$ *and such that*

$$\lambda_2^{opt}(p(\tau)) = 0 \quad \textit{for} \quad \tau \leq 0,$$
$$\lambda_1^{opt}(p(\tau)), \lambda_2^{opt}(p(\tau)) > 0 \quad \textit{for} \quad \tau > 0.$$

Moreover, we define gradual critical conditions *if* $\lambda^{opt}(p(\tau))$ *depend continuously on* τ*.*

Tightening the constraint that limits the active EFM (let us call it the first constraint) most, will force the growth-maximising micro-organism to switch already at these conditions. This is proven in full generality for any flux-maximising metabolic network in Subsection 6 below. Tightening the other constraint will, however, delay the switch. In many experiments these 'critical conditions' correspond to a concentration of a growth-limiting substrate. This critical concentration at the switch will decrease (resp. increase) if the first (resp. second) constraint is tightened. Therefore this is the first quantitative marker that can be used to determine which enzyme pool is affected most by the perturbation.

At non-critical environmental conditions we can still draw some conclusions. If both constrained enzyme pools are tightened equally by the experimental perturbation, we know exactly what happens to points on the flux-versus-growth rate plot. A growth-maximising micro-organism will keep the same ratio of its fluxes versus its growth rate, although both decrease due to the perturbation, see Theorem 11.

It is more difficult to understand fully what happens when we are at non-critical conditions and the perturbation affects one pool more than the other. However, note that biological data is often well-described by models in which enzyme saturations are kept fixed. This is equivalent to the assumption that internal metabolite concentrations vary only mildly over different growth conditions. Fixing these saturations would for example give rise to straight acetate excretion lines in overflow metabolism, exactly as found in the literature (***Basan et al.***, 2015). We therefore use this assumption to make a qualitative prediction of how experimental perturbations affect points on the fermentation flux curve, while further environmental conditions are kept fixed. Tightening the constraint that bounds respiration most (the first constraint) will decrease the growth rate more than it will decrease the fermentation flux. Tightening the other constraint will decrease fermentation more than the growth rate, and tightening both constraints equally will decrease fermentation and growth rate proportionally. We give the details in Subsection 6.

The critical substrate concentrations are affected differently for tightening the different constraints

In the next Theorem we will focus on the metabolic switch from a pure strategy to a mixed strategy. We pick the exact environmental conditions at which the microorganism switches from one to two EFMs, see Definition 2, and then tighten one of the constraints. Tightening the constraint that bounds the active EFM more than the inactive EFM (in the overflow metabolism examples this is the first constraint) will force the organism to choose the mixed strategy already at these conditions. Tightening the other constraint will postpone the mixing of EFMs.

Theorem 7. *Consider again the following maximisation problem*

$$\max_{\boldsymbol{x}^I,\lambda}\left\{\lambda_1+\lambda_2 \mid \lambda_i \geq 0,\ \boldsymbol{D}(\boldsymbol{x}^E,\boldsymbol{x}^I)\cdot\lambda \leq \begin{bmatrix}1\\1\end{bmatrix}\right\}, \tag{7}$$

where $\boldsymbol{D} = \left[\boldsymbol{d}^1(\boldsymbol{x}^E,\boldsymbol{x}^I),\quad \boldsymbol{d}^2(\boldsymbol{x}^E,\boldsymbol{x}^I)\right]$ *is the cost vector matrix. Assume that the cost vectors are in mixable position, that* $\boldsymbol{x}^E$ *is such that the global maximum has* $\lambda_2 = 0$ *and additionally that at this optimum* $\frac{\mathrm{d}(\lambda_1+\lambda_2)}{\mathrm{d}x^i} = 0$ *for each* $i \in \boldsymbol{I}$*. Then the maximisation problem*

$$\max_{\boldsymbol{x}^I,\lambda}\left\{\lambda_1+\lambda_2 \mid \lambda_i \geq 0,\ \boldsymbol{D}(\boldsymbol{x}^E,\boldsymbol{x}^I)\cdot\lambda \leq \begin{bmatrix}1-\nu\\1\end{bmatrix}\right\}, \tag{8}$$

with $\nu > 0$ *has a global maximum at* $\lambda_2 > 0$*.*

Proof. For given external conditions $\boldsymbol{x}^E$ we have a set of optimal internal concentrations $\boldsymbol{x}^I$ and an optimal set of fluxes λ. Let us call the initial external concentrations $\boldsymbol{x}_0^E$ and the corresponding optima $\boldsymbol{x}_0^I$ and $\lambda(\boldsymbol{x}_0)$. We will keep $\boldsymbol{x}_0^E$ fixed throughout, and are interested in the change of the optimal λ under tightening constraints. By assumption, $\lambda_2(\boldsymbol{x}_0) = 0$ and $\left.\frac{\mathrm{d}(\lambda_1(\boldsymbol{x}_0)+\lambda_2(\boldsymbol{x}_0))}{\mathrm{d}x^i}\right|_{\boldsymbol{x}_0} = 0$ for $i \in \boldsymbol{I}$.

To exploit our knowledge about this zero derivative, we must use that the two-component cost vectors $\boldsymbol{d}^1, \boldsymbol{d}^2$ depend smoothly on all internal metabolite concentrations $(x_1, \dots x_n)$ in a neighbourhood of $\boldsymbol{x}_0^I$. The dependence on $\boldsymbol{x}$ in the cost vectors appears in the rate kinetics functions $f_j(\boldsymbol{x})$. Since these depend smoothly on $\boldsymbol{x}$, so do the cost vectors.

Let $\lambda = \lambda(\boldsymbol{x}_0)$ denote the solution to $\boldsymbol{D}(\boldsymbol{x}_0)\cdot\lambda = \boldsymbol{1}$. Solving this explicitly for λ_1 and λ_2 yields

$$\lambda_1(\boldsymbol{x}_0) = \frac{d_2^2(\boldsymbol{x}_0) - d_1^2(\boldsymbol{x}_0)}{\det \boldsymbol{D}}, \quad \lambda_2(\boldsymbol{x}_0) = \frac{-d_2^1(\boldsymbol{x}_0) + d_1^1(\boldsymbol{x}_0)}{\det \boldsymbol{D}}.$$

Using that $\boldsymbol{d}^1$ is a diagonal vector, we find for $i \in \boldsymbol{I}$ that

$$0 = \frac{\mathrm{d}}{\mathrm{d}x_i}\left(\lambda_1(\boldsymbol{x}_0)+\lambda_2(\boldsymbol{x}_0)\right) = \frac{\frac{\partial d_1^1(\boldsymbol{x}_0)}{\partial x_i}(d_2^2(\boldsymbol{x}_0) - d_1^1(\boldsymbol{x}_0)) + \frac{\partial d_2^1(\boldsymbol{x}_0)}{\partial x_i}(d_1^1(\boldsymbol{x}_0) - d_1^2(\boldsymbol{x}_0))}{\det \boldsymbol{D}}.$$

Recognizing this as a dot product, we find that $\frac{\partial}{\partial x_i}\boldsymbol{d}^1(\boldsymbol{x}_0) \perp \begin{bmatrix}d_2^2 - d_1^1\\ d_1^1 - d_1^2\end{bmatrix} \perp \boldsymbol{d}^1 - \boldsymbol{d}^2$, where we again used that $\boldsymbol{d}^1$ is diagonal. Because we do this analysis in two dimensions, we get

$$\frac{\partial}{\partial x_i}\boldsymbol{d}^1(\boldsymbol{x}_0) = c\left(\boldsymbol{d}^2(\boldsymbol{x}_0) - \boldsymbol{d}^1(\boldsymbol{x}_0)\right) \tag{9}$$

for a suitable nonzero $c \in \mathbb{R}$. We conclude therefore that the derivative of the first cost vector with respect to *all possible* changes in the internal metabolite concentrations points in the direction of the second cost vector, see ***Figure 1***.

Expanding d_1^1 around $\boldsymbol{x}_0$,

$$d_1^1(\boldsymbol{x}) = d_1^1(\boldsymbol{x}_0) + \left[(\boldsymbol{x} - \boldsymbol{x}_0) \cdot \nabla_{\boldsymbol{x}} d_1^1(\boldsymbol{x}_0)\right] + \left[(\boldsymbol{x} - \boldsymbol{x}_0) \cdot (H(d_1^1)(\boldsymbol{x}_0) \cdot (\boldsymbol{x} - \boldsymbol{x}_0))\right] + \cdots, \tag{10}$$

where

$$H(d_1^1) = \begin{bmatrix} \frac{\partial^2 d_1^1}{\partial x_1^2} & \cdots & \frac{\partial^2 d_1^1}{\partial x_1 \partial x_m} \\ \vdots & \ddots & \vdots \\ \frac{\partial^2 d_1^1}{\partial x_m \partial x_1} & \cdots & \frac{\partial^2 d_1^1}{\partial x_m^2} \end{bmatrix}. \tag{11}$$

Using (9), and setting $\boldsymbol{x} = \boldsymbol{x}_0 + \boldsymbol{\delta x}$, with $\boldsymbol{\delta x}^E = \boldsymbol{0}$ (i.e, we only vary the internal concentrations), we get

$$\boldsymbol{d}^1(\boldsymbol{x}) = \boldsymbol{d}^1(\boldsymbol{x}_0) + \left[c\boldsymbol{\delta x} \cdot \left(\boldsymbol{d}^2(\boldsymbol{x}_0) - \boldsymbol{d}^1(\boldsymbol{x}_0)\right)\right] + \left[\boldsymbol{\delta x} \cdot (H(\boldsymbol{d}^1)(\boldsymbol{x}_0) \cdot \boldsymbol{\delta x})\right] + \cdots, \tag{12}$$

where we have used slightly abusive notation for the vector-valued Hessian:

$$H(\boldsymbol{d}^1) = \begin{bmatrix} \frac{\partial^2 \boldsymbol{d}^1}{\partial x_1^2} & \cdots & \frac{\partial^2 \boldsymbol{d}^1}{\partial x_1 \partial x_m} \\ \vdots & \ddots & \vdots \\ \frac{\partial^2 \boldsymbol{d}^1}{\partial x_m \partial x_1} & \cdots & \frac{\partial^2 \boldsymbol{d}^1}{\partial x_m^2} \end{bmatrix}.$$

Equation (33) describes the feasible positions of the first cost vector under different internal metabolite concentrations.

Let us now consider the new maximisation problem, given by Equation (8). This gives a new diagonal for the constraint box $s[1-\nu, 1]^T$ with $s \in [0, 1]$. Note that the generalisations of Definition 1 and Lemmas 3 and 4 remain valid, because we can simply rescale the new constraints and cost vectors to get the unit box again. There are now two options for the new maximum of $\lambda_1 + \lambda_2$, either $\lambda_2 = 0$ or $\lambda_2 > 0$. According to Theorem 6 the first option ($\lambda_2 = 0$) will only be optimal if there is a new set of metabolite concentrations for which $\boldsymbol{d}^1$ is on the new diagonal. Therefore we distinguish two strategies to find a global optimum: 1) adjust the metabolite concentrations such that the first cost vector will be on the new diagonal and 2) take a combination of the cost vectors to end up on the new diagonal. For option 2) we at least know one feasible combination of cost vector positions, which are the old positions $\boldsymbol{d}^1(\boldsymbol{x}_0)$ and $\boldsymbol{d}^2(\boldsymbol{x}_0)$. The intersection of this combination of two cost vectors with the new diagonal will be along the line

$$\boldsymbol{d}^1(\boldsymbol{x}_0) + m(\boldsymbol{d}^2(\boldsymbol{x}_0) - \boldsymbol{d}^1(\boldsymbol{x}_0)) \qquad m \in [0, 1]. \tag{13}$$

Option 1) is a little bit more complicated because it involves the Hessian $H(\boldsymbol{d}^1)$. It was recently shown that for practically any rate law, sums of the form $\sum_k \frac{c_k}{f_k(\boldsymbol{x})}$ are strictly convex in the optimum (***Planque et al.***, 2017). The cost vectors $\boldsymbol{d}^1(\boldsymbol{x})$ and $\boldsymbol{d}^2(\boldsymbol{x})$ have exactly this form. Therefore, for each component of the cost vector, the Hessian is strictly positive definite: $\boldsymbol{\delta x} \cdot (H(d_k^1)(\boldsymbol{x}_0) \cdot \boldsymbol{\delta x}) > 0$.

We will now use this result to prove that the intersection obtained by option 1) is always further from the origin than the intersection obtained by option 2), thereby proving that the new global maximum will have $\lambda_2 > 0$. In order to do this we define a linear map ω that assigns a real number to the cost vector $\boldsymbol{d}^1(\boldsymbol{x})$. This number is equal to the length of the projection of the cost vector to a vector perpendicular to $\boldsymbol{d}^2(\boldsymbol{x}_0) - \boldsymbol{d}^1(\boldsymbol{x}_0)$. We can write this down as

$$\omega\left(\begin{bmatrix} a \\ b \end{bmatrix}\right) = \begin{bmatrix} d_2^2(\boldsymbol{x}_0) - d_2^1(\boldsymbol{x}_0) \\ d_1^1(\boldsymbol{x}_0) - d_1^2(\boldsymbol{x}_0) \end{bmatrix} \cdot \begin{bmatrix} a \\ b \end{bmatrix} =: \begin{bmatrix} v \\ w \end{bmatrix} \cdot \begin{bmatrix} a \\ b \end{bmatrix}, \tag{14}$$

for which it is only important that v and w are positive. This is true because the vectors are in mixable position. This linear map is equal-valued for all the points on the line between

the two original cost vectors:

$$\omega\left(\boldsymbol{d}^1(\boldsymbol{x}_0) + m(\boldsymbol{d}^2(\boldsymbol{x}_0) - \boldsymbol{d}^1(\boldsymbol{x}_0))\right) = \begin{bmatrix} v \\ w \end{bmatrix} \cdot \begin{bmatrix} d_1^1(\boldsymbol{x}_0) \\ d_2^1(\boldsymbol{x}_0) \end{bmatrix} = v d_1^1(\boldsymbol{x}_0) + w d_2^1(\boldsymbol{x}_0). \tag{15}$$

The linear map applied to the feasible positions of $\boldsymbol{d}^1$ (Equation (33)) yields

$$\begin{aligned} \omega\left(\boldsymbol{d}^1(\boldsymbol{x})\right) &= v d_1^1(\boldsymbol{x}_0) + w d_2^1(\boldsymbol{x}_0) + \begin{bmatrix} v \\ w \end{bmatrix} \cdot \left[\boldsymbol{\delta x} \cdot (H(\boldsymbol{d}^1)(\boldsymbol{x}_0) \cdot \boldsymbol{\delta x})\right] + \cdots, \\ &= v d_1^1(\boldsymbol{x}_0) + w d_2^1(\boldsymbol{x}_0) + \left[\boldsymbol{\delta x} \cdot (H(v d_1^1 + w d_2^1)(\boldsymbol{x}_0) \cdot \boldsymbol{\delta x})\right] + \cdots. \end{aligned}$$

Since $v, w > 0$, the function $v d_1^1(\boldsymbol{x}) + w d_2^1(\boldsymbol{x})$ is still strictly convex near its optimum and it has an optimum exactly at $\boldsymbol{x}_0$, since

$$\begin{aligned} \frac{\partial}{\partial x_i}\left(v d_1^1(\boldsymbol{x}) + w d_2^1(\boldsymbol{x})\right)\Big|_{\boldsymbol{x}=\boldsymbol{x}_0} &= \frac{\partial}{\partial x_i}\left(\left(d_2^2(\boldsymbol{x}_0) - d_2^1(\boldsymbol{x}_0)\right) d_1^1(\boldsymbol{x}) + \left(d_1^1(\boldsymbol{x}_0) - d_1^2(\boldsymbol{x}_0)\right) d_2^1(\boldsymbol{x})\right), \\ &= \begin{bmatrix} d_2^2(\boldsymbol{x}_0) - d_2^1(\boldsymbol{x}_0) \\ d_1^1(\boldsymbol{x}_0) - d_1^2(\boldsymbol{x}_0) \end{bmatrix} \cdot \frac{\partial}{\partial x_i} \boldsymbol{d}^1(\boldsymbol{x}) \\ &= \begin{bmatrix} d_2^2(\boldsymbol{x}_0) - d_2^1(\boldsymbol{x}_0) \\ d_1^1(\boldsymbol{x}_0) - d_1^2(\boldsymbol{x}_0) \end{bmatrix} \cdot \left(\boldsymbol{d}^2(\boldsymbol{x}_0) - \boldsymbol{d}^1(\boldsymbol{x}_0)\right) \\ &= 0. \end{aligned}$$

This strict convexity means that the extra term $(\boldsymbol{\delta x} \cdot (H(v d_1^1 + w d_2^1)(\boldsymbol{x}_0) \cdot \boldsymbol{\delta x}))$ is positive, so we get the following inequality for the intersection points with the diagonal for the pure and the mixed strategy

$$\omega\left(\boldsymbol{d}^1(\boldsymbol{x})\right) > \omega\left(\boldsymbol{d}^1(\boldsymbol{x}_0) + m(\boldsymbol{d}^2(\boldsymbol{x}_0) - \boldsymbol{d}^1(\boldsymbol{x}_0))\right). \tag{16}$$

To be able to determine which of the two strategies, with $\lambda_2 = 0$ or $\lambda_2 > 0$ yields higher fitness, we invoke Corollary 5 and study the points of intersection with the new diagonal $[1 - \nu, 1]^\intercal$. The strategy with intersection closest to the origin then yields highest flux. The intersection point of a strategy with value $\lambda_2 = \lambda_2^*$ is $s[1 - \nu, 1]^\intercal$ for a suitable $s > 0$, and the s-value indicated by $s_{\lambda_2 = \lambda_2^*}$.

We can now easily show that $s_{\lambda_2 > 0} > s_{\lambda_2 = 0}$, so that we will have $\lambda_2 > 0$ in the global maximum for the new maximisation problem. This follows from

$$\begin{aligned} s_{\lambda_2=0}\left((1-\nu)v + w\right) = \left(\omega\left(s_{\lambda_2=0}(1-\nu, 1)\right)\right. &= \omega\left(\boldsymbol{d}^1(\boldsymbol{x})\right) > \omega\left(\boldsymbol{d}^1(\boldsymbol{x}_0) + m(\boldsymbol{d}^2(\boldsymbol{x}_0) - \boldsymbol{d}^1(\boldsymbol{x}_0))\right) \\ &= \omega\left(s_{\lambda_2>0}(1-\nu, 1)\right) = s_{\lambda_2>0}\left((1-\nu)v + w\right), \end{aligned}$$

so that $s_{\lambda_2=0} > s_{\lambda_2>0}$. Combined with Lemma 4 this implies that tightening the first constraint will lead to a combination at environmental conditions where a pure strategy was first used. □

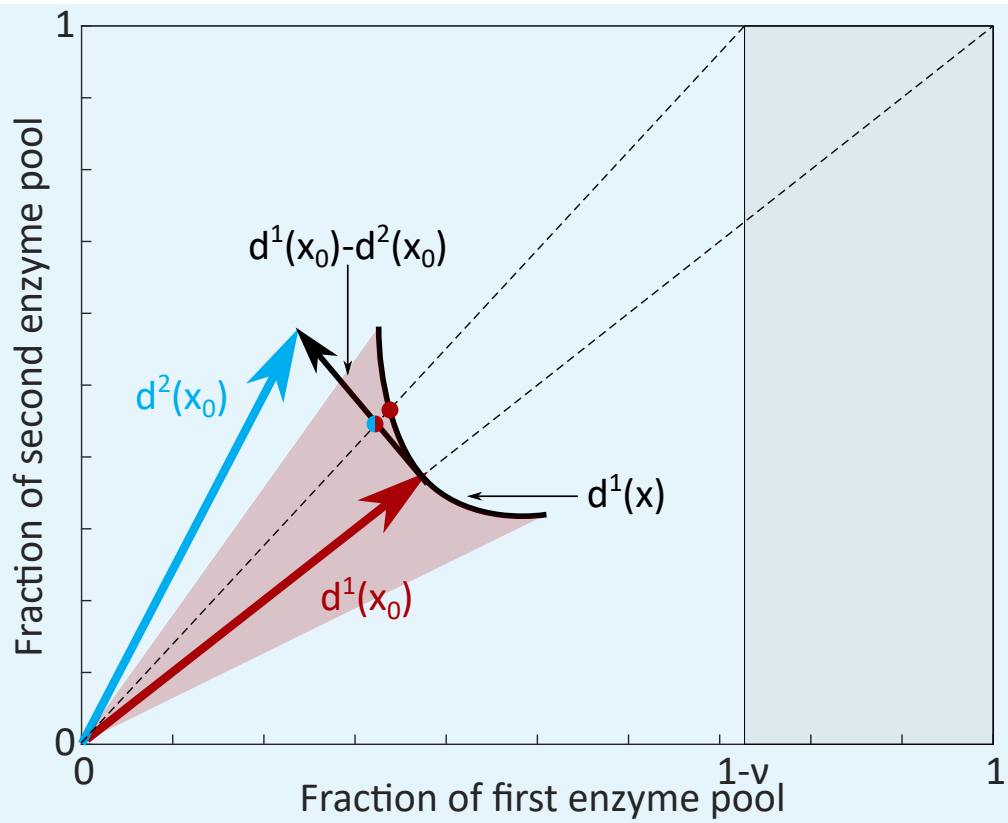

Appendix 6 Figure 1. A visualisation of the proof of Theorem 7. At the critical environmental conditions, the derivative of cost vector $\boldsymbol{d}^1(x)$ with respect to the metabolite concentrations is in the direction of $\boldsymbol{d}^2(x)$. Moreover, the curve of feasible positions for $\boldsymbol{d}^1(x)$ lies completely outside the triangle spanned by the two cost vectors. This means that upon tightening of the first constraint, and thereby changing the diagonal of the constraint box, a mixture of EFMs will give rise to a higher flux than pure use of the red EFM.

Corollary 8. *Assume that we choose the gradual critical environmental conditions (following Definition 2). Experimentally tightening the constraint that limits the active EFM will force the microorganism to mix EFMs already at these conditions.*

Proof. According to the proof of Theorem 1, a growth maximising wildtype microorganism will solve the following maximisation problem

$$\max_{\boldsymbol{x}^I,\lambda} \left\{ \lambda_1 + \lambda_2 \mid \lambda_i \geq 0,\ \boldsymbol{D}(\boldsymbol{x}^E, \boldsymbol{x}^I) \cdot \boldsymbol{\lambda} \leq \begin{bmatrix} 1 \\ 1 \end{bmatrix} \right\}, \tag{17}$$

where $\boldsymbol{D} = \begin{bmatrix} \boldsymbol{d}^1(\boldsymbol{x}^E, \boldsymbol{x}^I) & \boldsymbol{d}^2(\boldsymbol{x}^E, \boldsymbol{x}^I) \end{bmatrix}$ is the cost vector matrix. The definition of gradual critical conditions (Definition 2) states that there is a path $p(\tau)$ with $p(0) = x^E_{cr}$ that leads from pure EFM usage $\lambda_2 = 0$ to mixed EFM usage $\lambda_2 > 0$. We will here prove that we are then in the situation to which Theorem 7 applies.

We start by showing that the optimal internal concentration $\boldsymbol{x}^I$ for vectors in mixable positions depend continuous differentiable on the external concentrations $\boldsymbol{x}^E$. Recall that these optima are calculated by setting the derivatives to zero of the objective function $\lambda_1 + \lambda_2$ with respect to all internal concentrations. By Lemma 4 we know that this is equivalent to setting the derivatives of $\beta(\boldsymbol{x}^E, \boldsymbol{x}^I)$ to zero, where β is determined by $t(\boldsymbol{x}^E, \boldsymbol{x}^I)\boldsymbol{d}^1(\boldsymbol{x}^E, \boldsymbol{x}^I) + (1 - t(\boldsymbol{x}^E, \boldsymbol{x}^I))\boldsymbol{d}^2(\boldsymbol{x}^E, \boldsymbol{x}^I) = [\beta(\boldsymbol{x}^E, \boldsymbol{x}^I), \beta(\boldsymbol{x}^E, \boldsymbol{x}^I)]^T$. In the optimum we have

$$\nabla_{\boldsymbol{x}^I} \beta(\boldsymbol{x}^E, \boldsymbol{x}^I) = \boldsymbol{0}. \tag{18}$$

We can now apply the Implicit Function Theorem (IFT) if the Hessian $H(t\boldsymbol{d}^1 + (1-t))\boldsymbol{d}^2)$ is invertible. Since the Hessian is positive definite (***Planque et al.***, 2017), it is also invertible. The IFT then states that there are continuous differentiable functions around the optimum that describe the optimal internal concentrations as a function of the external concentrations, $\boldsymbol{x}^I(\boldsymbol{x}^E)$.

Since the cost vectors are smooth functions of the internal and external concentrations, we may define a continuously differentiable map $\bar{\boldsymbol{d}}$ of τ by setting

$$\bar{\boldsymbol{d}}(\tau) := \boldsymbol{d}(p(\tau), \boldsymbol{x}^I(p(\tau))).$$

We also know that for all $\tau > 0$ we have a mixed strategy, i.e. $\lambda_2 > 0, \lambda_1 > 0$. This will only be optimal when the vectors are in mixable position (Theorem 6). Since the vectors in mixable position form a set in $\mathbb{R}^2$. Since the continuous map $\bar{\boldsymbol{d}}(\tau)$ maps the open interval $(0,1)$ in this closed set, we know that it will map the limit point $\tau = 0$ into this set or its boundary. The boundary of the set consists of those combinations of vectors for which $d_1^1 = d_1^2$ or $d_2^1 = d_2^2$. In that case, there will be no global optimum, so that the assumption of gradual critical environmental conditions would be violated. Hence, the vectors at $\tau = 0$ must still be in mixable position.

Since the objective function $\lambda_1 + \lambda_2$ is also a continuous differentiable function of the concentrations, these will also vary smoothly with $\boldsymbol{x}^E$. This gives us a continuous differentiable map $(\lambda_1 + \lambda_2)(p(\tau))$ from the path p.

For all $\tau > 0$ we know that $(\lambda_1 + \lambda_2)(p(\tau))$ is the optimal flux value, and $\nabla_{\boldsymbol{x}^I}(\lambda_1 + \lambda_2)\big|_{\tau>0} = 0$. So, the continuous map $\nabla_{\boldsymbol{x}^I}(\lambda_1 + \lambda_2)(\tau) = 0$ is zero throughout the open interval $(0,1)$, but therefore also has to be zero on the limit point.

We conclude that at $\tau = 0$, the cost vectors are in mixable position, $\lambda_2 = 0$ is a global optimum (by definition of critical), and $\nabla_{\boldsymbol{x}^I}(\lambda_1 + \lambda_2)\big|_{\tau=0} = 0$. We therefore are in the exact situation to which Theorem 7 applies. Experimentally tightening the constraint that inhibits the active EFM λ_1 most is now equivalent to changing the constraint in the maximisation problem to $\boldsymbol{D}(\boldsymbol{x}^E, \boldsymbol{x}^I) \cdot \lambda \leq \begin{bmatrix} 1-\nu \\ 1 \end{bmatrix}$. The theorem now tells us that the new global optimum will have $\lambda_2 > 0$ and therefore the microorganism will mix EFMs already at these, formerly critical, conditions. □

The effect of perturbations on points in the flux versus growth rate plane

Theorem 9. *Consider the maximisation problem as in Equation (7) at fixed external $\boldsymbol{x}_0^E$ and internal $\boldsymbol{x}_0^I$ metabolite concentrations and assume that we have two cost vectors in mixable position. We consider the situation in which we tighten the first constraint, i.e. we solve the following maximisation problem*

$$\max_{\boldsymbol{x}^I, \lambda} \left\{ \lambda_1 + \lambda_2 \mid \lambda_i \geq 0,\ \boldsymbol{D}(\boldsymbol{x}_0^E, \boldsymbol{x}_0^I) \cdot \lambda \leq \begin{bmatrix} 1-\nu \\ 1 \end{bmatrix} \right\}, \tag{19}$$

for $\nu \in [0,1]$. Then the flux through the second EFM versus growth rate ($\mu = \lambda_1 + \lambda_2$) at these concentrations $\boldsymbol{x}_0$ will follow a piecewise linear path to the origin:

$$(\mu(\nu), \lambda_2(\nu))_{\boldsymbol{x}_0} = \begin{cases} \frac{1}{\det(\boldsymbol{D})} \left(d_1^1 - d_2^1 + d_2^2 - d_1^2 + \nu\left(d_2^1 - d_2^2\right), d_1^1 - d_2^1 + \nu d_2^1\right) & \text{if } \nu \leq 1 - \frac{d_1^2}{d_2^2}, \\ \left(\frac{1-\nu}{d_1^2}, \frac{1-\nu}{d_1^2}\right) & \text{if } \nu > 1 - \frac{d_1^2}{d_2^2}. \end{cases} \tag{20}$$

Proof. We have two vectors in mixable position, so Lemma 3 states that the flux λ is described by the equality $\boldsymbol{D} \cdot \lambda = [1-\nu, 1]^T$. We therefore invert $\boldsymbol{D}$ to get an expression for the λ's.

$$\begin{bmatrix} \lambda_1 \\ \lambda_2 \end{bmatrix} = \frac{1}{\det(\boldsymbol{D})} \begin{bmatrix} d_2^2 & -d_1^2 \\ -d_2^1 & d_1^1 \end{bmatrix} \cdot \begin{bmatrix} 1-\nu \\ 1 \end{bmatrix} = \frac{1}{\det(\boldsymbol{D})} \begin{bmatrix} d_2^2 - d_1^2 - \nu d_2^2 \\ -d_2^1 + d_1^1 + \nu d_2^1 \end{bmatrix},$$

Note that we must have nonnegative fluxes $\lambda_i > 0$. This constrains the values of ν in which a combination of the EFMs will be chosen:

$$0 \leq \lambda_1 = \frac{1}{\det(\boldsymbol{D})} \left(d_2^2 - d_1^2 - \nu d_2^2\right) \quad \Rightarrow \quad \nu \leq 1 - \frac{d_1^2}{d_2^2}.$$

With $\nu > 1 - \frac{d_1^2}{d_2^2}$ the vectors are not in mixable position anymore, so that the optimal solution will involve only the second EFM and solve the inequality

$$\lambda_2 \begin{bmatrix} d_1^2 \\ d_2^2 \end{bmatrix} \leq \begin{bmatrix} 1-\nu \\ 1 \end{bmatrix} \quad \Rightarrow \quad \lambda_2 = \frac{1-\nu}{d_1^2}.$$

For smaller ν, we find

$$\lambda_2 = \frac{1}{\det(\boldsymbol{D})} \left(d_1^1 - d_2^1 + \nu d_2^1\right),$$
$$\mu = \lambda_1 + \lambda_2 = \frac{1}{\det(\boldsymbol{D})} \left(d_1^1 - d_2^1 + d_2^2 - d_1^2 + \nu \left(d_2^1 - d_2^2\right)\right)$$

□

The following theorem is proved in an identical fashion.

Theorem 10. *Consider the maximisation problem as in Equation (7) at fixed external $\boldsymbol{x}_0^E$ and internal $\boldsymbol{x}_0^I$ metabolite concentrations and assume that we have two cost vectors in mixable position. We consider the situation in which we tighten the second constraint, i.e. we solve the following maximisation problem*

$$\max_{\boldsymbol{x}^I, \lambda} \left\{ \lambda_1 + \lambda_2 \mid \lambda_i \geq 0,\ \boldsymbol{D}(\boldsymbol{x}_0^E, \boldsymbol{x}_0^I) \cdot \lambda \leq \begin{bmatrix} 1 \\ 1-\nu \end{bmatrix} \right\}, \tag{21}$$

for $\nu \in [0, 1]$. Then the flux through the second EFM versus growth rate ($\mu = \lambda_1 + \lambda_2$) at these concentrations $\boldsymbol{x}_0$ will follow a two-part linear path to the origin:

$$(\mu(\nu), \lambda_2(\nu))_{\boldsymbol{x}_0} = \begin{cases} \frac{1}{\det(\boldsymbol{D})} \left(d_1^1 - d_2^1 + d_2^2 - d_1^2 + \nu \left(d_1^2 - d_1^1\right), d_1^1 - d_2^1 - \nu d_1^1\right) & \text{if } \nu \leq 1 - \frac{d_2^1}{d_1^1} \\ \left(\frac{1-\nu}{d_2^1}, 0\right) & \text{if } \nu > 1 - \frac{d_2^1}{d_1^1} \end{cases} \tag{22}$$

Theorem 11. *Consider the maximisation problem as in Equation (7) at fixed external $\boldsymbol{x}_0^E$ but arbitrary internal $\boldsymbol{x}^I$ metabolite concentrations and assume that we have two cost vectors in mixable position. We consider the situation in which we tighten both constraints, i.e. we solve the following maximisation problem*

$$\max_{\boldsymbol{x}^I, \lambda} \left\{ \lambda_1 + \lambda_2 \mid \lambda_i \geq 0,\ \boldsymbol{D}(\boldsymbol{x}_0^E, \boldsymbol{x}^I) \cdot \lambda \leq \begin{bmatrix} 1-\nu \\ 1-\nu \end{bmatrix} \right\}, \tag{23}$$

for different values of $\nu \in [0, 1]$. Then the flux through the second EFM versus growth rate ($\mu = \lambda_1 + \lambda_2$), at these concentrations $\boldsymbol{x}_0^E$, will follow a straight line to the origin

$$(\mu(\nu), \lambda_2(\nu))_{\boldsymbol{x}} = \frac{1}{\det(\boldsymbol{D})}((d_1^1 - d_2^1 + d_2^2 - d_1^2)(1-\nu), (d_1^1 - d_2^1)(1-\nu)) \qquad \text{for } 0 \leq \nu \leq 1. \tag{24}$$

Proof. Note that we can not just copy the proof of Theorem 9 because this theorem makes a stronger statement. The internal concentrations are not fixed, such that the cost vectors can, in principle, adapt to the experimental perturbations. We will show however, that the optimal solutions at all ν will have the same internal concentrations.

We have two vectors in mixable position, so Lemma 3 states that the flux λ is described by the equality $\boldsymbol{D}(\boldsymbol{x}) \cdot \lambda = [1-\nu, 1]^T$. We therefore invert $\boldsymbol{D}$ again to get an expression for the λ's.

$$\begin{bmatrix} \lambda_1 \\ \lambda_2 \end{bmatrix} = \frac{1}{\det(\boldsymbol{D})} \begin{bmatrix} d_2^2 & -d_1^2 \\ -d_2^1 & d_1^1 \end{bmatrix} \cdot \begin{bmatrix} 1-\nu \\ 1-\nu \end{bmatrix} = \frac{1}{\det(\boldsymbol{D})} \begin{bmatrix} (d_2^2 - d_1^2)(1-\nu) \\ (d_1^1 - d_2^1)(1-\nu) \end{bmatrix}, \tag{25}$$

but note that the cost vector components d_i^j are still dependent on the internal metabolite concentrations $\boldsymbol{x}^I$. We therefore want to maximize the sum of fluxes

$$O(\boldsymbol{x}) = \lambda_1 + \lambda_2 = \frac{1}{\det(\boldsymbol{D})}(d_1^1(\boldsymbol{x}) - d_2^1(\boldsymbol{x}) + d_2^2(\boldsymbol{x}) - d_1^2(\boldsymbol{x}))(1-\nu)$$

over all x. In the optimum all derivatives of this objective function with respect to $\boldsymbol{x}^I$ must be zero, but it is easy to see that this is independent of the value of ν:

$$\nabla_{\boldsymbol{x}^I} O = (1-\nu)\nabla_{\boldsymbol{x}^I}\left(\frac{1}{\det(\boldsymbol{D})}\left(d_1^1(\boldsymbol{x}) - d_2^1(\boldsymbol{x}) + d_2^2(\boldsymbol{x}) - d_1^2(\boldsymbol{x})\right)\right) = 0.$$

Therefore, the vector of internal concentrations $\boldsymbol{x}_0^I$ that was optimal at $\nu = 0$ will also be the maximum for all other values of ν. The cost vector components will therefore not change and Equation (25) shows us that all fluxes, and therefore also μ, scale with $1-\nu$. □

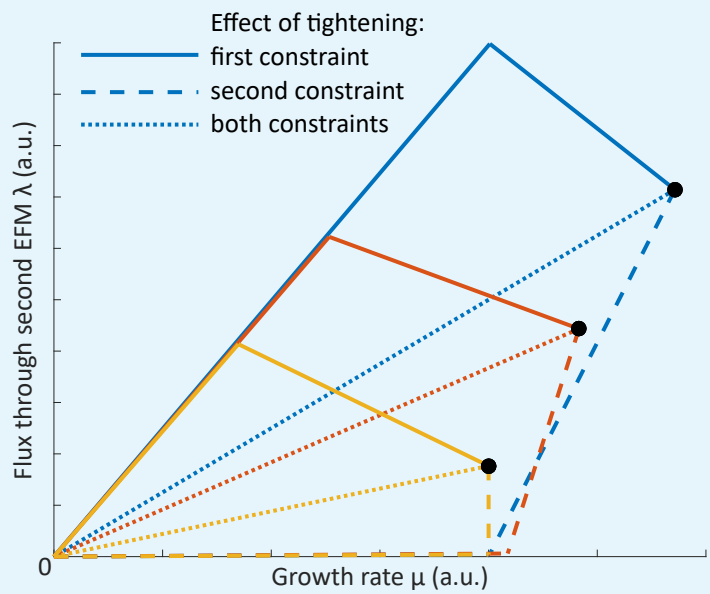

Appendix 6 Figure 2. Illustration of the conclusions from Theorems 9, 10 and 11. Tightening different constraints will have different effects on the growth rate μ and the flux through one of the EFMs, such that we could in principle infer from data which constraint was affected most.

The results from Theorem 9, 10 and 11 are summarized in ***Figure 2***. The following corollary is a biological interpretation of these Theorems, and is summarized in ***Figure 3***.

Corollary 12. *Consider a growth maximising wildtype microorganism that shows a metabolic shift from one EFM to two EFMs when the growth rate is increased. The biomass flux through the added EFM can be plotted against the growth rate. A point on this line $(\mu_{WT}, \lambda_{2,WT})$ is associated to a vector of metabolite concentrations $\boldsymbol{x}$. If these metabolite concentrations are kept fixed while*

the constrained enzyme pools are experimentally tightened, this will affect the coordinates of the point in the following way.

1. *tightening the first constraint will increase the ratio ($\frac{\lambda_2}{\mu}$) until 1, which corresponds to a pure EFM*
2. *tightening the second constraint will decrease the ratio ($\frac{\lambda_2}{\mu}$) to zero*
3. *tightening both constraints proportionally will keep the ratio ($\frac{\lambda_2}{\mu}$) constant while the growth rate is decreased to zero*

Proof. According to the proof of Theorem 1 a growth maximising microorganism will solve the maximisation problem of Equation (4). After the metabolic shift to two EFMs Theorem 6 states that the cost vectors must be in mixable positions. We can then plot the flux through the second EFM λ_2 versus the growth rate which is proportional to the total biomass flux $\lambda_1 + \lambda_2$. This brings us in the situation in which the Theorems 9, 10 and 11 apply.

Theorem 9 states that tightening the first constraint will move points on the (μ, λ_2)-line over the following path

$$(\mu(\nu), \lambda_2(\nu))_{\boldsymbol{x}_0} = \begin{cases} \frac{1}{\det(\boldsymbol{D})}\left(d_1^1 - d_2^1 + d_2^2 - d_1^2 + \nu\left(d_2^1 - d_2^2\right), d_1^1 - d_2^1 + \nu d_2^1\right) & \text{if } \nu \leq 1 - \frac{d_1^2}{d_2^2}, \\ \left(\frac{1-\nu}{d_1^2}, \frac{1-\nu}{d_1^2}\right) & \text{if } \nu > 1 - \frac{d_1^2}{d_2^2}. \end{cases} \tag{26}$$

The ratio $\frac{\lambda_2}{\mu}$ is obviously 1 in the second part of this path. In the first part of the path we see that μ decreases since $(d_2^1 - d_2^2) < 0$ because the vectors are in mixable position, and λ_2 increases. Therefore the ratio $\frac{\lambda_2}{\mu}$ increases.

Theorem 10 states that tightening the second constraint will move points on the (μ, λ_2)-line over the following path

$$(\mu(\nu), \lambda_2(\nu))_{\boldsymbol{x}_0} = \begin{cases} \frac{1}{\det(\boldsymbol{D})}\left(d_1^1 - d_2^1 + d_2^2 - d_1^2 + \nu\left(d_1^2 - d_1^1\right), d_1^1 - d_2^1 - \nu d_1^1\right) & \text{if } \nu \leq 1 - \frac{d_2^1}{d_1^1}, \\ \left(\frac{1-\nu}{d_2^1}, 0\right) & \text{if } \nu > 1 - \frac{d_2^1}{d_1^1}. \end{cases} \tag{27}$$

The ratio $\frac{\lambda_2}{\mu}$ is 0 in the second part of this path. In the first part of the path the ratio is

$$\frac{\lambda_2}{\mu} = \frac{d_1^1 - d_2^1 - \nu d_1^1}{d_1^1 - d_2^1 + d_2^2 - d_1^2 + \nu\left(d_1^2 - d_1^1\right)},$$

such that

$$\begin{aligned} \frac{\partial}{\partial \nu}\frac{\lambda_2}{\mu} &= \frac{-\left(d_1^1 - d_2^1 + d_2^2 - d_1^2 + \nu\left(d_1^2 - d_1^1\right)\right)d_1^1 - \left(d_1^1 - d_2^1 - \nu d_1^1\right)\left(d_1^2 - d_1^1\right)}{\left(d_1^1 - d_2^1 + d_2^2 - d_1^2 + \nu\left(d_1^2 - d_1^1\right)\right)^2}, \\ &= \frac{-\left(d_1^1 - d_2^1 + d_2^2 - d_1^2\right)d_1^1 - \left(d_1^1 - d_2^1\right)\left(d_1^2 - d_1^1\right) + \nu d_1^1\left(d_1^2 - d_1^1\right) - \nu\left(d_1^2 - d_1^1\right)d_1^1}{\left(d_1^1 - d_2^1 + d_2^2 - d_1^2 + \nu\left(d_1^2 - d_1^1\right)\right)^2}, \\ &= \frac{-\left(d_1^1 - d_2^1 + d_2^2 - d_1^2\right)d_1^1 - \left(d_1^1 - d_2^1\right)\left(d_1^2 - d_1^1\right)}{\left(d_1^1 - d_2^1 + d_2^2 - d_1^2 + \nu\left(d_1^2 - d_1^1\right)\right)^2}, \\ &= \frac{-d_2^2 d_1^1 + d_2^1 d_1^2}{\left(d_1^1 - d_2^1 + d_2^2 - d_1^2 + \nu\left(d_1^2 - d_1^1\right)\right)^2}, \\ &\leq \frac{-d_2^2 d_1^1 + d_2^2 d_1^1}{\left(d_1^1 - d_2^1 + d_2^2 - d_1^2 + \nu\left(d_1^2 - d_1^1\right)\right)^2}, \\ &= 0. \end{aligned}$$

Theorem 11 states that tightening both constraints will move points on the (μ, λ_2)-line over the following path

$$(\mu(\nu), \lambda_2(\nu))_{\boldsymbol{x}} = \frac{1}{\det(\boldsymbol{D})}((d_1^1 - d_2^1 + d_2^2 - d_1^2)(1-\nu), (d_1^1 - d_2^1)(1-\nu)) \qquad \text{for } 0 \leq \nu \leq 1. \tag{28}$$

The ratio $\frac{\lambda_2}{\mu} = \frac{(d_1^1 - d_2^1)(1-\nu)}{(d_1^1 - d_2^1 + d_2^2 - d_1^2)(1-\nu)} = \frac{d_1^1 - d_2^1}{d_1^1 - d_2^1 + d_2^2 - d_1^2}$ is of course constant. □

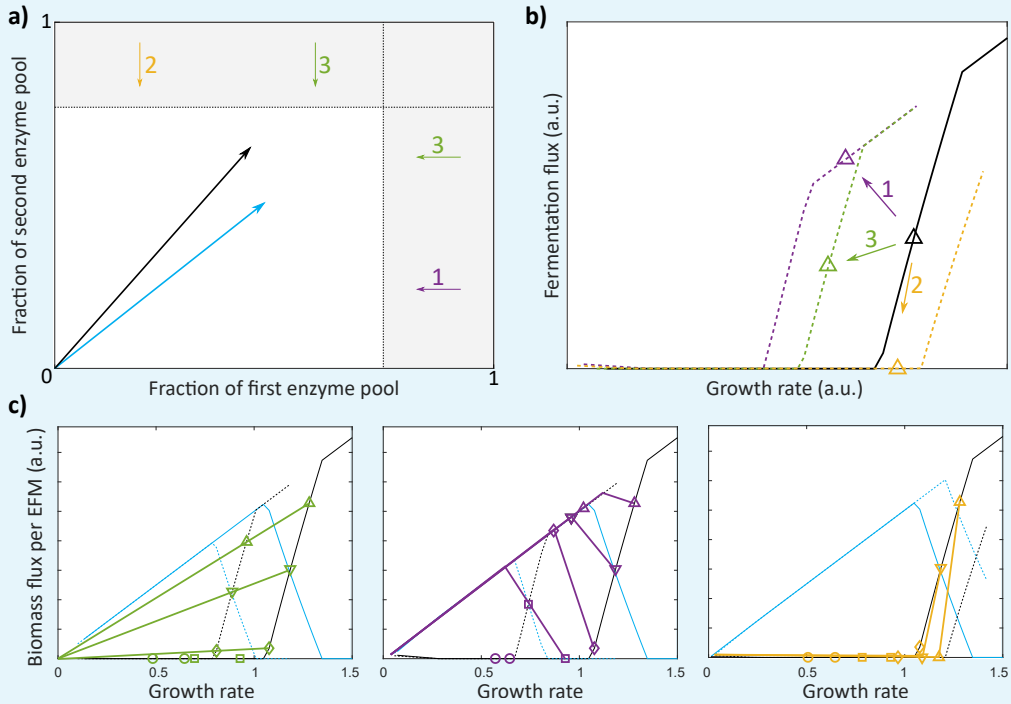

Appendix 6 Figure 3. a) We used our core model of overflow metabolism to find out the effect of tightening only the first (purple), only the second (orange) or both constraints (green). **b)** The black triangle indicates the optimal growth rate and fermentation flux predicted by the unperturbed model at certain environmental conditions. Tightening of the constraints will force the fermentation flux over growth rate ratio to increase (first constraint), to decrease (second) or to remain constant (both). **c)** We did the same analysis for three different environmental conditions. Solid (green, purple, orange) lines show the effect of tightening (both, the first, the second) constraint(s).

Remark:

We have not yet addressed the situation in which one constraint is tightened more than the other, say we have to solve the following maximisation problem

$$\max_{\boldsymbol{x}^I, \lambda} \left\{ \lambda_1 + \lambda_2 \mid \lambda_i \geq 0,\ \boldsymbol{D}(\boldsymbol{x}_0^E, \boldsymbol{x}^I) \cdot \lambda \leq \begin{bmatrix} 1-\nu_1 \\ 1-\nu_2 \end{bmatrix} \right\}, \tag{29}$$

with $\nu_1 \neq \nu_2$. To find out what will happen to the ratio $\frac{\lambda_2}{\mu}$ we can just combine two of the situations in Corollary 12. We take the smallest of ν_1 and ν_2, let us say $\nu_1 < \nu_2$. If we solve the maximisation problem $\boldsymbol{D}(\boldsymbol{x}_0^E, \boldsymbol{x}^I) \cdot \lambda \leq \begin{bmatrix} 1-\nu_1 \\ 1-\nu_1 \end{bmatrix}$, the ratio of λ_2 and μ will remain constant. Subsequently we tighten the second constraint further until it is at $1-\nu_2$, i.e. $\boldsymbol{D}(\boldsymbol{x}_0^E, \boldsymbol{x}^I) \cdot \lambda \leq \begin{bmatrix} 1-\nu_1 \\ 1-\nu_2 \end{bmatrix}$. This will decrease the ratio. Overall we will thus see an increase of $\frac{\lambda_2}{\mu}$. In this manner all experimental perturbations that tighten the constraints can be analysed.

Appendix 7

The effect on overflow metabolism of a non-lethal dose of chloramphenicol

In the previous section we have focused on experimental perturbations that result in a tightening of a constraint ($\sum_i w_i e_i \leq C$). These perturbations either affect the right side of the constraint, e.g. by taking up a volume in the cytosol when the constraint is a limited cytosolic volume, or by affecting all enzymatic costs on the left side by the same factor, e.g. by the synthesis of an 'average' dummy protein. There are however also perturbations that have a kinetic effect on one specific enzyme, e.g. by reducing the maximal catalytic rate k_{cat}. In this section we show that for chloramphenicol the results in ***Appendix 6*** are still valid. Other kinetic inhibitions should be treated on a case by case basis.

Recall the definition of a cost vector

$$d_k^i(\boldsymbol{x}) = \sum_{j=1}^{M} C_k^j \frac{V_j^i}{f_j(\boldsymbol{x})}. \tag{30}$$

We model the effect of chloramphenicol by a inhibition of the ribosome, say e_r, which will result in the multiplication of its activity by a number $\alpha < 1$, i.e. $f_r(\boldsymbol{x}) \to \alpha f_r(\boldsymbol{x})$. Note that we model the ribosome as an enzyme that catalyses the synthesis of proteins. We need to prove a new theorem for this situation.

Theorem 13. *Consider the following maximisation problem*

$$\max_{\boldsymbol{x}^I, \lambda} \left\{ \lambda_1 + \lambda_2 \mid \lambda_i \geq 0,\ \boldsymbol{D}(\boldsymbol{x}^E, \boldsymbol{x}^I) \cdot \lambda \leq \begin{bmatrix} 1 \\ 1 \end{bmatrix} \right\}, \tag{31}$$

where $\boldsymbol{D} = \left[\boldsymbol{d}^1(\boldsymbol{x}^E, \boldsymbol{x}^I), \quad \boldsymbol{d}^2(\boldsymbol{x}^E, \boldsymbol{x}^I) \right]$ *is the cost vector matrix. Assume that the cost vectors are in mixable position, that* $\boldsymbol{x}^E$ *is such that the global maximum has* $\lambda_2 = 0$ *and additionally that at this optimum* $\frac{\mathrm{d}(\lambda_1+\lambda_2)}{\mathrm{d}x^i}|_{x=x_0} = 0$ *for each* $i \in I$*. Then the maximisation problem*

$$\max_{\boldsymbol{x}^I, \lambda} \left\{ \lambda_1 + \lambda_2 \mid \lambda_i \geq 0,\ \tilde{\boldsymbol{D}}(\boldsymbol{x}^E, \boldsymbol{x}^I) \cdot \lambda \leq \begin{bmatrix} 1 \\ 1 \end{bmatrix} \right\}, \tag{32}$$

with $\tilde{\boldsymbol{D}} = \begin{bmatrix} d_1^1(\boldsymbol{x}^E, \boldsymbol{x}^I) + C_1^r \tilde{\rho} & d_1^2(\boldsymbol{x}^E, \boldsymbol{x}^I) + C_1^r \tilde{\rho} \\ d_2^1(\boldsymbol{x}^E, \boldsymbol{x}^I) & d_2^2(\boldsymbol{x}^E, \boldsymbol{x}^I) \end{bmatrix}$ *has a global maximum at* $\lambda_2 > 0$.

Proof. The beginning of the proof of Theorem 7 can be applied here, such that we end up with an equation for the feasible positions of $\boldsymbol{d}^1$:

$$\boldsymbol{d}^1(\boldsymbol{x}) = \boldsymbol{d}^1(\boldsymbol{x}_0) + \left[c\boldsymbol{\delta x} \cdot \left(\boldsymbol{d}^2(\boldsymbol{x}_0) - \boldsymbol{d}^1(\boldsymbol{x}_0) \right) \right] + \left[\boldsymbol{\delta x} \cdot (H(\boldsymbol{d}^1)(\boldsymbol{x}_0) \cdot \boldsymbol{\delta x} \right] + \cdots. \tag{33}$$

In the new maximisation problem of Equation (32) both cost vectors will be shifted. For these new cost vectors we have two options for the maximum of $\lambda_1 + \lambda_2$: $\lambda_2 = 0$ or $\lambda_2 > 0$, again leading to the strategies 1) adjust the metabolite concentrations such that the first cost vectors will be on the diagonal, and 2) take a combination of the new cost vectors to end up on the diagonal. For option 2) we have at least one feasible combination, i.e. using the old metabolite concentrations. This will give an intersection with the diagonal somewhere along the line

$$\boldsymbol{d}^1(\boldsymbol{x}_0) + \begin{bmatrix} C_1^r \tilde{\rho} \\ 0 \end{bmatrix} + m(\boldsymbol{d}^2(\boldsymbol{x}_0) + \begin{bmatrix} C_1^r \tilde{\rho} \\ 0 \end{bmatrix} - \boldsymbol{d}^1(\boldsymbol{x}_0) - \begin{bmatrix} C_1^r \tilde{\rho} \\ 0 \end{bmatrix}) = \boldsymbol{d}^1(\boldsymbol{x}_0) + \begin{bmatrix} C_1^r \tilde{\rho} \\ 0 \end{bmatrix} + m(\boldsymbol{d}^2(\boldsymbol{x}_0) - \boldsymbol{d}^1(\boldsymbol{x}_0)).$$

The linear map of Equation (14) can now again be applied to both options, yielding

$$\omega\left(\boldsymbol{d}^1(\boldsymbol{x}_0)+\begin{bmatrix}C_1^r\tilde{\rho}\\0\end{bmatrix}+m(\boldsymbol{d}^2(\boldsymbol{x}_0)-\boldsymbol{d}^1(\boldsymbol{x}_0))\right)=\begin{bmatrix}v\\w\end{bmatrix}\cdot\begin{bmatrix}d_1^1(\boldsymbol{x}_0)+C_1^r\tilde{\rho}\\d_2^1(\boldsymbol{x}_0)\end{bmatrix}=v(d_1^1(\boldsymbol{x}_0)+C_1^r\tilde{\rho})+wd_2^1(\boldsymbol{x}_0),$$

for the second strategy (mixture), and

$$\begin{aligned}\omega\left(\boldsymbol{d}^1(\boldsymbol{x})+\begin{bmatrix}C_1^r\tilde{\rho}\\0\end{bmatrix}\right)&=v\left(d_1^1(\boldsymbol{x}_0)+C_1^r\tilde{\rho}\right)+wd_2^1(\boldsymbol{x}_0)+\begin{bmatrix}v\\w\end{bmatrix}\cdot\left[\boldsymbol{\delta x}\cdot(H(\boldsymbol{d}^1)(\boldsymbol{x}_0)\cdot\boldsymbol{\delta x})\right]+\cdots,\\&=v\left(d_1^1(\boldsymbol{x}_0)+C_1^r\tilde{\rho}\right)+wd_2^1(\boldsymbol{x}_0)+\left[\boldsymbol{\delta x}\cdot(H(vd_1^1+wd_2^1)(\boldsymbol{x}_0)\cdot\boldsymbol{\delta x})\right]+\cdots.\end{aligned}$$

for the first strategy (pure solution). We can, as we did in Theorem 7, use the convexity of the cost vectors to see that

$$\omega\left(\boldsymbol{d}^1(\boldsymbol{x}_0)+\begin{bmatrix}C_1^r\tilde{\rho}\\0\end{bmatrix}+m(\boldsymbol{d}^2(\boldsymbol{x}_0)-\boldsymbol{d}^1(\boldsymbol{x}_0))\right)<\omega\left(\boldsymbol{d}^1(\boldsymbol{x})+\begin{bmatrix}C_1^r\tilde{\rho}\\0\end{bmatrix}\right)$$

The intersection of a strategy with the diagonal can be paramaterized by suitable positive scalars $s_{\lambda_2=0}, s_{\lambda_2>0}$, such that $s_{\lambda_2=0}[1,1]^\intercal=\boldsymbol{d}^1(\boldsymbol{x})+\begin{bmatrix}C_1^r\tilde{\rho}\\0\end{bmatrix}$ and $s_{\lambda_2>0}[1,1]^\intercal=\boldsymbol{d}^1(\boldsymbol{x}_0)+\begin{bmatrix}C_1^r\tilde{\rho}\\0\end{bmatrix}+m(\boldsymbol{d}^2(\boldsymbol{x}_0)-\boldsymbol{d}^1(\boldsymbol{x}_0))$. It is now easy to see that

$$\begin{aligned}s_{\lambda_2=0}(v+w)=\omega\left(s_{\lambda_2=0}[1,1]^\intercal\right)=\omega\left(\boldsymbol{d}^1(\boldsymbol{x})+\begin{bmatrix}C_1^r\tilde{\rho}\\0\end{bmatrix}\right)&>\omega\left(\boldsymbol{d}^1(\boldsymbol{x}_0)+\begin{bmatrix}C_1^r\tilde{\rho}\\0\end{bmatrix}+m(\boldsymbol{d}^2(\boldsymbol{x}_0)-\boldsymbol{d}^1(\boldsymbol{x}_0))\right)\\&=\omega\left(s_{\lambda_2>0}[1,1]^\intercal\right)=s_{\lambda_2>0}(v+w),\end{aligned}$$

so that $s_{\lambda_2=0}>s_{\lambda_2>0}$. Combined with Lemma 4 this implies that the new maximisation problem will lead to a combination at environmental conditions where a pure strategy was first used.

□

The following corollary and theorem show how the addition of chloramphenicol affects overflow metabolism.

Corollary 14. *Assume that we choose the gradual critical environmental conditions (following Definition 2). We experimentally inhibit an enzyme that is part of the pool that inhibits the active EFM most, but which is used in both EFMs in the same amount. Say that the enzyme is inhibited in a linear fashion $f_i(\boldsymbol{x})\to\alpha f_i(\boldsymbol{x})$. This will force the microorganism to start mixing EFMs at these conditions.*

Proof. The multiplicative inhibition will increase the enzymatic cost for this reaction and Equation (30) will change to:

$$\tilde{d}_k^i(\boldsymbol{x})=\sum_{j\neq r}C_k^j\frac{V_j^i}{f_j(\boldsymbol{x})}+C_k^r\frac{V_r^i}{\alpha f_r(\boldsymbol{x})}.$$

Now write $\alpha=1-\beta$ with $\beta>0$, we can rewrite

$$\tilde{d}_k^i(\boldsymbol{x})=\sum_{j\neq r}C_k^j\frac{V_j^i}{f_j(\boldsymbol{x})}+C_k^r\frac{V_r^i}{f_r(\boldsymbol{x})}+C_k^r\frac{\beta}{1-\beta}\frac{V_r^i}{f_r(\boldsymbol{x})}=d_k^i(\boldsymbol{x})+C_k^r\frac{\beta}{1-\beta}\frac{V_r^i}{f_r(\boldsymbol{x})}=d_k^i(\boldsymbol{x})+C_k^r\rho\frac{V_r^i}{f_r(\boldsymbol{x})},$$

where $\rho=\frac{\beta}{1-\beta}=\frac{1-\alpha}{\alpha}$. In the case of the ribosome we can make a simplifying assumption. The synthesis of proteins is essential for cell growth and will therefore be present in every EFM that leads to cell synthesis. Moreover, we normalized the cost vector such that it show the costs to produce one unit cell synthesis flux; therefore, the flux through the protein

synthesis reaction V_r will be approximately equal in both EFMs, i.e. $V_r^2 \approx V_r^1$. Hence, if we use $\rho \frac{V_r^2}{f_r(\boldsymbol{x})} = \rho \frac{V_r^2}{f_r(\boldsymbol{x})} \approx \tilde{\rho}$ we can write

$$\tilde{d}_k^i(\boldsymbol{x}) = d_k^i(\boldsymbol{x}) + C_k^r \tilde{\rho}.$$

The costs of both EFMs will thus increase with the same amount in the direction of both constraints. This is exactly the situation in which Theorem 13 applies.

It can be shown that the other conditions necessary for Theorem 13 are also satisfied using the same proof as for Corollary 8 □

We can also prove statements analogous to Corollary 12 in the case of chloramphenicol addition.

Theorem 15. *Consider a growth maximising wildtype microorganism that shows a metabolic shift from one EFM to two EFMs when the growth rate is increased. The cell synthesis flux through the added EFM can be plotted against the growth rate. A point on this line $(\mu_{WT}, \lambda_{2,WT})$ is associated to a vector of metabolite concentrations $\boldsymbol{x}$. If, at those metabolite concentrations, an enzyme is inhibited in a linear fashion $f_i(\boldsymbol{x}) \to \alpha f_i(\boldsymbol{x})$ for some $\alpha > 0$, this will affect the coordinates of the point in the following way:*

1. *inhibiting an enzyme in the first constrained pool will increase the ratio $(\frac{\lambda_2}{\mu})$ until 1, which corresponds with the usage of one EFM*
2. *inhibiting an enzyme in the second constrained pool will decrease the ratio $(\frac{\lambda_2}{\mu})$ to zero*
3. *inhibiting an enzyme which forms an equal part of both constraints will keep the ratio $(\frac{\lambda_2}{\mu})$ constant while the growth rate is decreased to zero*

Proof. In ***Appendix 6*** we explicitly solved the growth rate maximisation in the case of overflow metabolism:

$$\lambda_1(\boldsymbol{x}_0) = \frac{d_2^2(\boldsymbol{x}_0) - d_1^2(\boldsymbol{x}_0)}{\det \boldsymbol{D}}, \quad \lambda_2(\boldsymbol{x}_0) = \frac{d_1^1(\boldsymbol{x}_0) - d_2^1(\boldsymbol{x}_0)}{\det \boldsymbol{D}}.$$

The cost vectors however change as described above (recall the monotonous relation between $\tilde{\rho}$ and the perturbation $1 - \alpha$), resulting in the following λ's:

$$\lambda_1(\boldsymbol{x}_0) = \frac{d_2^2(\boldsymbol{x}_0) + C_2^r\tilde{\rho} - d_1^2(\boldsymbol{x}_0) - C_1^r\tilde{\rho}}{\det \tilde{\boldsymbol{D}}}, \quad \lambda_2(\boldsymbol{x}_0) = \frac{d_1^1(\boldsymbol{x}_0) + C_1^r\tilde{\rho} - d_2^1(\boldsymbol{x}_0) - C_2^r\tilde{\rho}}{\det \tilde{\boldsymbol{D}}}.$$

Note that these expressions for λ_i are only valid when the cost vectors are in mixable position. The expression for the fraction $\frac{\lambda_2}{\mu}$ becomes

$$\frac{\lambda_2}{\mu} = \frac{\lambda_2}{\lambda_1 + \lambda_2} = \frac{d_1^1 - d_2^1 + C_1^r\tilde{\rho} - C_2^r\tilde{\rho}}{d_2^2 - d_2^1 - d_1^2 + d_1^1}. \tag{34}$$

In the regime where the cost vectors are in mixable position, the denominator is positive and the derivatives with respect to $\tilde{\rho}$ can be calculated from Equation (34). Because of the monotonous relation between $\tilde{\rho}$ and the perturbation $1 - \alpha$, we indeed see that the fraction $\frac{\lambda_2}{\mu}$ increases, decreases or is stable when the inhibited enzyme is in the first, second or both constrained pools respectively.

Eventually the cost vectors will however not be in mixable position anymore. When the inhibited enzyme is part of the first constrained pool, then $\boldsymbol{d}^2(\boldsymbol{x})$ will become lower-diagonal. In that case $\frac{\lambda_2}{\mu}$ becomes one. The inhibition of an enzyme of the second pool forces $\boldsymbol{d}^1(\boldsymbol{x})$ to become above-diagonal, in which case only $d^1(\boldsymbol{x})$ will be used and $\frac{\lambda_2}{\mu} = 0$. When the enzyme is an equal part of both constrained pools, we can mimic the proof of Theorem 11 to show that the fraction will remain constant. □

Appendix 8

Experimental evidence of a small number of EFMs

We here reinterpret two sets of experimental data that indicate the usage of only a small number of EFMs. Firstly, we show that the substrate uptake fluxes increase proportionally to the growth rate over a large range of environmental conditions for many organisms, Figure in main text. We will explain in Subsection 8 that this is a strong indication that there is only 1 active EFM in that range of conditions.

Secondly, Stosch et al (***von Stosch et al.***, 2016) performed a variance analysis on measured flux data of *S. cerevisiae* and *P. pastoris*. They could explain 90 percent of the *S. cerevisiae* data by using only 10 EFMs and 99 percent of the *P. pastoris* data with only 6 EFMs. Note that this analysis was performed on a dataset compiled out of different experiments, using several strains and different conditions. That the major part of variance across these conditions can be explained from only 6-10 EFMs provides an upper bound on the number of active EFMs at the separate conditions.

Combining these two analyses, we estimate the number of active EFMs to be in the order of 1 to 3.

Constant growth rate over flux ratios indicate the use of only one EFM

In a metabolic network with a substrate uptake flux v_1 and a flux of interest v_r we define the substrate r-yield as the ratio $Y^r = v_r/v_1$. Within the ith EFM, this value Y^i is fixed, since all ratios between flux values are fixed within an EFM.

A combination of EFMs, as in Equation (1), will lead to a yield that combines the yields of the pure EFMs:

$$Y = \frac{\lambda_1 Y^1 + \cdots + \lambda_F Y^F}{\lambda_1 + \cdots + \lambda_F}, \text{ where } \lambda_i \geq 0. \tag{35}$$

The λ_i factors are dependent on metabolite concentrations and will therefore vary between different experiments. A cell that uses a combination of EFMs is thus expected to show different yields at different conditions.

We observe a constant ratio of growth rate over substrate uptake fluxes (glucose and oxygen) in a large range of environmental conditions, see data in the main text. The growth rate μ is proportional to the cell synthesis flux, which is now the flux of interest v_r. The most straightforward explanation of the experimental data is that only one EFM is used in this range of conditions (only one nonzero λ_i in (1)). Within one EFM, the flux through the EFM can change, but the ratio between fluxes remain constant, leading to the straight line before the critical growth rate.

After the critical growth rate, an additional EFM is clearly used, since the ratio of growth rate over uptake flux changes. Note that the glucose yield decreases rapidly after this critical growth rate, which can be expected because of the onset of overflow metabolism.

An alternative hypothesis is that a combination of EFMs is used in exactly the same proportion in the full range of growth rates below the critical growth rate. This however seems rather unlikely because metabolite concentrations will influence the λ-factors, thereby changing the relative use of active EFMs which would lead to changed growth rate over flux ratios.

A more probable alternative is the use of a combination in which one EFM is very dominant. Fluctuations in the use of the other EFMs could then become smaller than the experimental noise, hence showing constant yields. A last alternative could be the simultaneous use of a combination of EFMs with exactly the same flux ratios. In that case, a combination would not give rise to a changing yield. We however see that both the glucose

and the oxygen yield are very constant. Therefore, both of these yields should be the same in the separate EFMs. These last two alternatives cannot be completely excluded, but will only result in small deviations from our theory.

Appendix 9

Core model of overflow metabolism

The core model of mixed behaviour which was referred to in the main text was made using Matlab (Matlab-files are supplemented). In this model we picked an objective reaction: the reaction towards biomass. The flux through the objective reaction was fixed and we minimized the substrate concentration, which is analogous to the actual selective pressure in a chemostat. The Matlab programs (which are attached to the SI) return the optimal concentrations of all metabolites and enzymes.

The cost vectors that were shown in the main text in ***Figure 3*** were calculated at the optimal metabolite concentrations. We calculated the necessary fractions of the constrained enzyme pools to obtain one unit of enzyme flux, according to the definition of a cost vector given in Equation (3). The alternative positions of the cost vectors are obtained by starting from the optimal concentrations and then vary one of the intracellular metabolite concentrations.

Overflow metabolism

The rate equations used were all of the form $v_i = e_i f_i(\boldsymbol{x})$. In the overflow metabolism model we used a transporter (v_{tr}) reaction, a respiration (v_r) and a fermentation (v_f) reaction and a biomass v_{BM} reaction. The details can be found in the SBML-file. More detailed results of this model can be found in Figure ***Figure 1***.

A remarkable aspect of this simulation is that the flux through respiration is before the critical growth rate not proportional to the concentration of respiration proteins. This behaviour is found in various experiments (***Goel et al.***, 2015; ***Canelas et al.***, 2011) and cannot be explained by current models that fix enzyme saturations. In fact, the presence of two separate enzyme constraints causes this behaviour: the respiration proteins (which are part of the first constrained pool) are expressed at low growth rates to reduce the cost of the EFM for the transporter pool by reducing product inhibition by keeping internal glucose levels low.

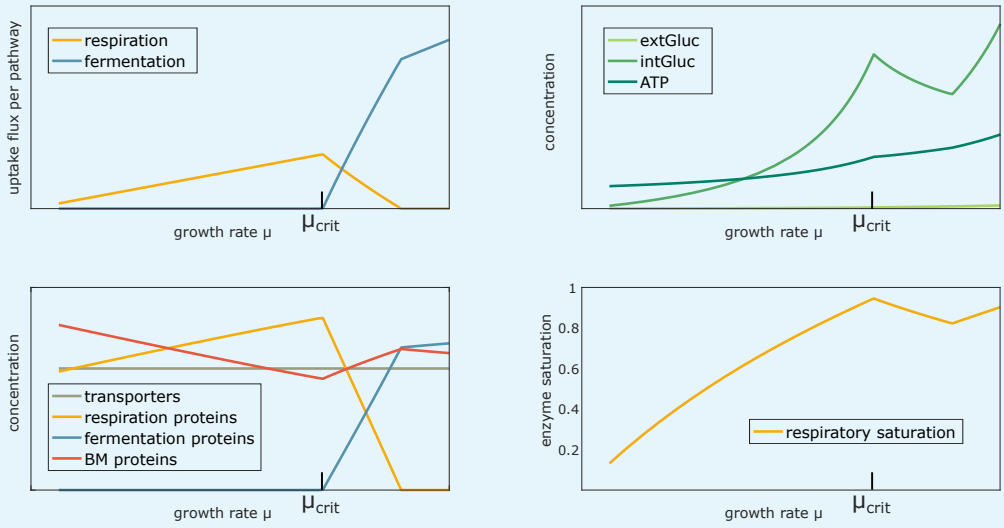

Appendix 9 Figure 1. Additional model results from our core model of overflow metabolism. The flux through respiration increases proportionally to the growth rate until the critical growth rate μ_{crit}, after which respiratory flux decreases and fermentation flux increases. In our model, the membrane constraint is always saturated, indicated by a constant level of transporters. Respiratory proteins do increase slightly with growth rate, but not with the same factor as respiratory flux, indicating an increase in their activity: indeed, internal glucose levels increase up to the critical growth rate.

Appendix 10

Finding EFMs that co-consume carbon sources

We showed that the number of active EFMs in a growth-maximising micro-organism is bounded by the number of active enzymatic constraints. Since the number of these constraints seems to be low in many experiments, we asked if it could be optimal to co-consume multiple carbon sources given this small number of constraints. We therefore investigated if there is an EFM that by itself consumes two or even three carbon sources and found EFMs for all combinations that we have tested.

The Python- and Matlab-program that we used to find these EFMs is attached to the SI. It works by first performing a Flux Balance Analysis on a genome-scale metabolic network. In this FBA, the exchange reactions that are set reversible are either essential (trace elements, oxygen, ammonium) or the carbon sources of interested. This makes sure that the optimal solution of this FBA will use these carbon sources. Subsequently, the inactive reactions in the optimal solution are deleted from the network. The resulting smaller network is loaded into Matlab, where a package is used (***Terzer and Stelling***, 2008) to enumerate the EFMs. These EFMs are checked for co-consumption of the carbon sources.

Note that we find only *if* there is an EFM that co-consumes the carbon sources of interest, not how many EFMs exist that do this.

Appendix 11

Coconsumption experiment

Method

Strain information

All experiments were performed with *E. coli* strain MG1655.

Growth conditions

The medium employed was the N- C- minimal medium from Gutnick et al. (***Gutnick et al.***, 1969), which contains (per liter): K_2SO_4 (1 g), K_2HPO_4 (13.5 g), KH_2PO_4 (4.7 g), $MgSO_4{\cdot}7H_2O$ (0.1 g) and NaCl (2.5 g), supplemented with 20 mM NH_4Cl and thiamine (1mg). After adding saturating amounts of either a single carbon substrate or a combination of multiple (see ***Table 1***), the pH was set to 7.1 using KOH.

Appendix 11 Table 1. Carbon mixtures that have been used in combination with the N- C- minimal medium.

Glucose 0.4 % (w/v)	Mannose 20 mM	Maltose 20 mM	Succinate 15 mM	Xylose 20 mM	Abbr
x					G
	x				M
		x			L
			x		S
				x	X
		x	x		SL
	x	x			ML
		x		x	XL
			x	x	XS
	x		x		SM
		x	x	x	SLX
	x	x	x		SLM

Cells were seeded from a frozen glycerol stock into 5 ml liquid N-C- minimal medium +glucose and cultured in 30x115 mm conical tubes, shaking with 220 rpm at 37°C. During the subsequent 12 hours they were sequentially diluted into tubes with the desired medium, to achieve exponential growth and removal of undesired carbon. Then, depending on the specific growth rate in each condition, cells of the various cultures were diluted to different densities and 200 μl of each was transferred to a Greiner 96-well, flat bottom plate. The plate was kept shaking at 37°C and densities were measured at 600 nm using a Spectramax 384 plus (Molecular Devices). Cell densities were chosen such that 8 doublings could take place before growth in the plate could be detected. Every condition was represented by 10 micro-wells (i.e. technical replicates) during each experiment, to make sure enough volume was available for sampling. Samples were taken during growth, filtrated and stored at -20°C for further analysis. This experiment was performed in triplo, meaning that three biological replicates were done on separate days.

Carbon substrate uptake measurements

50μl of undiluted samples were analysed on their mannose, maltose, succinate and xylose content using HPLC (Shimadzo, LC-20AT) at a flow rate of 0.5 mL/min. Calibration samples were made for individual- and triple carbon sources in N-C- minimal medium, to determine the concentrations and validate good separation. Compounds were separated on an ROA-

Organic Acid H+ column (Phenomenex, Rezex) and detected using refractive index (Shimadzu, RID-10A) and UV-Vis (Shimadzu, SPD-20A).

Acetate concentrations were measured using an enzyme essay described by Smith et al. (***Smith et al.***, 1986). Samples were diluted either 10 or 100 times to stay in the linear range of NADH detection. The essay was conducted in a 96-well, flat bottom plate at 37°C and NADH oxidation was measured at 340 nm using a Spectramax 384 plus (Molecular Devices).

Data analysis

The three plate-reader experiments resulted in two types of data: OD measurements and HPLC (High Performance Liquid Chromatography) analyses of growth medium samples. The OD measurements were taken every 5 minutes during the full growth experiment and in total 104 growth medium samples were taken at different ODs for all conditions.

The OD measurements were analysed using Matlab. Background OD was subtracted and time windows of at least two hours were selected in which the natural logarithm of the measurements was sufficiently linear: ($R^2 > 0.95$). For these windows the specific growth rate ($\mu = \frac{1}{OD}\frac{dOD}{dt}$) was calculated and the maximum is reported below.

The HPLC analyses were normalized using a peak in the chromatogram that corresponded to a constant compound (phosphate) in the medium. Compound concentrations were calculated using a linear calibration curve that was made for all compounds. Since we were interested in the decrease of substrate concentration, rather than in the absolute value of these concentrations, the concentrations were normalized such that the t_0-concentration is equal to the intended initial concentration for that compound, thereby correcting for small pipetting errors.

Results

The calculated growth rates for all 12 conditions are summarized in ***Figure 1***. Data can be found in file: SI_growth_rates.txt. In almost all cases the growth rate increases or remains equal when an extra compound is added: only the combination of mannose and maltose leads to a lower growth rate than on maltose alone. The addition of succinate to the medium always leads to an increase in growth rate.

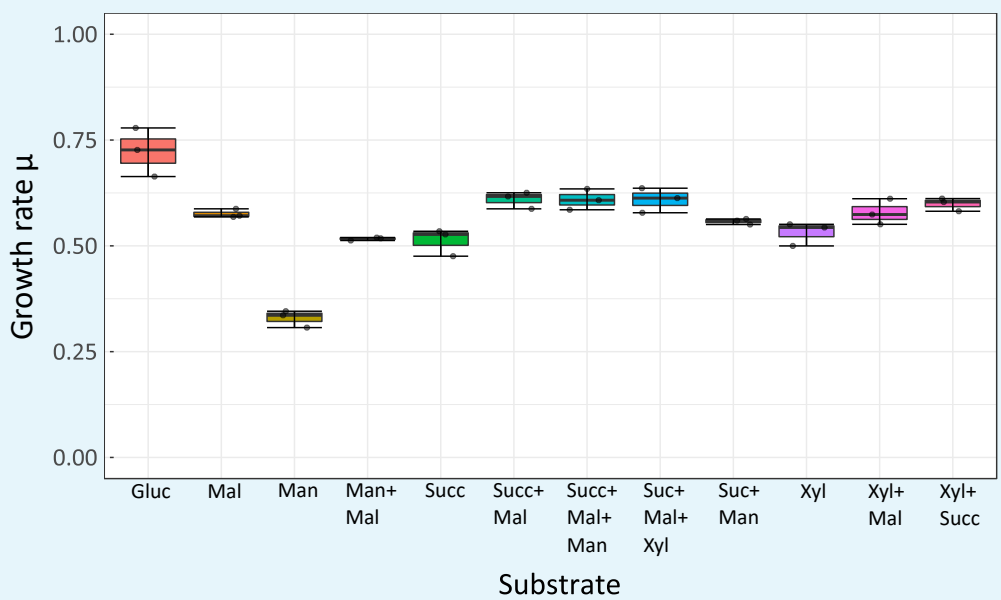

Appendix 11 Figure 1. Growth rates were measured for *E. coli* on media with combinations of glucose, maltose, mannose, succinate or xylose. Data from three biological replicates are shown. For each of these replicates, the growth rates from five technical replicates were averaged.

We determined for all conditions the mean specific uptake rate for all the compounds. The resulting data is shown in ***Table 2*** and the standard errors of the means are shown in ***Table 3***. This data can be found in SI_q_S_comp_cond.xlsx.

Appendix 11 Table 2. Mean specific uptake rate for the 12 conditions and 4 compounds in units: $\frac{\text{mmol}}{\text{OD}_{600}\cdot\text{hour}}$. The letters that indicate the conditions denote the available carbon sources in the medium: S=Succinate, L=maLtose, M=Mannose, X=Xylose, G=Glucose. The uptake rates were estimated from the fitted lines in ***Figure 2***.

	S	SL	M	ML	L	XL	G	XS	X	SLX	SM	SLM
Succinate	80.5	51.0	0.0	0.0	0.0	0.0	0.0	70.0	0.0	46.9	57.0	51.9
Maltose	0.0	59.2	0.0	32.5	71.5	42.0	0.0	0.0	0.0	35.8	0.0	30.2
Xylose	0.0	0.0	0.0	0.0	0.0	31.3	0.0	58.0	64.8	26.9	0.0	0.0
Mannose	0.0	0.0	33.1	27.8	0.0	0.0	0.0	0.0	0.0	0.0	19.0	25.3

Appendix 11 Table 3. Standard errors of the mean of specific uptake rate for the 12 conditions and 4 compounds in units: $\frac{\text{mmol}}{\text{OD}_{600}\cdot\text{hour}}$. The letters that indicate the conditions denote the available carbon sources in the medium: S=Succinate, L=maLtose, M=Mannose, X=Xylose, G=Glucose. Standard errors of the mean were calculated from the three biological replicates.

	S	SL	M	ML	L	XL	G	XS	X	SLX	SM	SLM
Succinate	8.6	4.1	0.0	0.0	0.0	0.0	0.0	10.1	0.0	6.6	9.5	7.0
Maltose	0.0	2.1	0.0	1.8	4.0	4.6	0.0	0.0	0.0	2.1	0.0	2.1
Xylose	0.0	0.0	0.0	0.0	0.0	1.8	0.0	2.9	1.9	2.2	0.0	0.0
Mannose	0.0	0.0	1.0	2.4	0.0	0.0	0.0	0.0	0.0	0.0	1.4	3.4

In Figure ***Figure 2*** we plot, for all conditions except for glucose, the relation between the optical density of cells in the sample and the concentrations of the compounds succinate, maltose, mannose and xylose. The dataset can be found in the file SI_OD_conc_per_cond.xlsx.

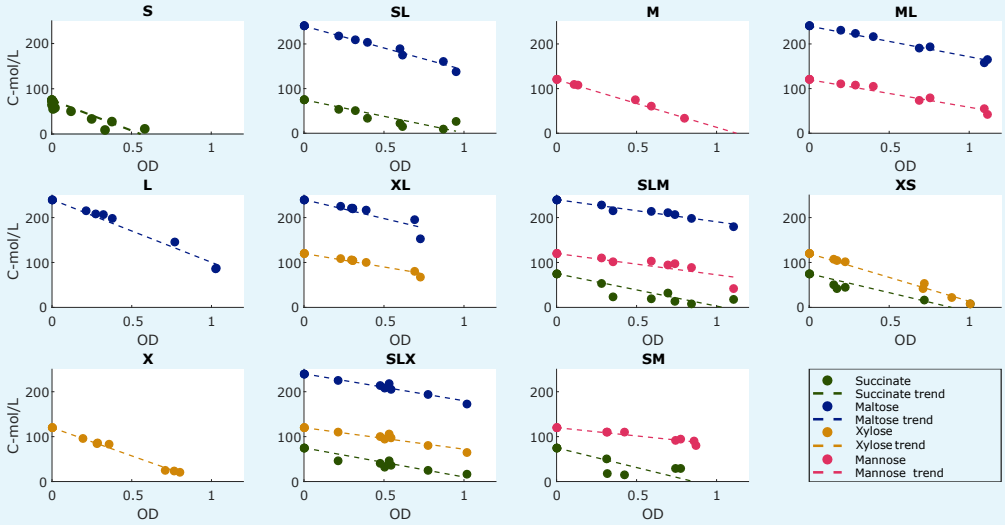

Appendix 11 Figure 2. During the growth experiments, the concentration of carbon sources was measured. The letters that indicate the conditions denote the available carbon sources in the medium: S=Succinate, L=maLtose, M=Mannose, X=Xylose, G=Glucose. We here show the decrease in these concentrations as the OD (Optical Density) of the culture increases. Data from three biological replicates was normalized for initial concentration and then shown together. The best linear approximation was calculated and shown by a dashed line.

Additional datasets

Dataset 1.

SI_growth_rates.txt Estimated growth rates from separate biological replicates.

Dataset 2.

SI_OD_conc_per_cond.xlsx For all different growth media, we include an excell-sheet. Shown are the measured concentrations of carbon sources (normalized for initial concentration), with the corresponding Optical Density (OD). The letters that indicate the conditions denote the available carbon sources in the medium: S=Succinate, L=maLtose, M=Mannose, X=Xylose, G=Glucose.

Dataset 3.

SI_q_S_comp_cond.xlsx Shown are the estimated uptake rates (mean and standard deviation) of different carbon sources (normalized for initial concentration) on the different growth media. The letters that indicate the conditions denote the available carbon sources in the medium: S=Succinate, L=maLtose, M=Mannose, X=Xylose, G=Glucose.